Pergamon

PII S0016-7037(02)00851-7

Laboratory simulation of an oxidizing perturbation in a deep granite environment

LAURENT TROTIGNON,[1,*] VALÉRIE MICHAUD,[1] JEAN-ERIC LARTIGUE,[1,2] JEAN-PAUL AMBROSI,[2] LAURENT EISENLOHR,[2,†]
LISE GRIFFAULT,[3] MICHEL DE COMBARIEU,[3] and SYLVIE DAUMAS[4]

[1]Commissariat à l'Energie Atomique, DEN/DED, Centre d'Etudes de Cadarache, 13108 Saint-Paul lez Durance, France
[2]CNRS, CEREGE, UMR 6635, Europôle Méditerranéen de l'Arbois, BP 80, 13545 Aix-en-Provence Cedex 04, France
[3]Andra, Service Hydro-Géochimie, Parc de la Croix Blanche, 1-7 rue Jean Monnet, 92298 Châtenay-Malabry Cedex, France
[4]Compagnie Française de Géothermie, Groupe BRGM, 117 avenue de Luminy, 13009 Marseille, France

Abstract—An experiment designed to study oxidizing perturbations in deep crystalline rock, a potential host for nuclear waste disposal, was conducted. This experiment simulated a fracture surface in contact with circulating groundwater, in which dissolved oxygen was injected periodically. Major physicochemical and biological parameters were monitored during this 1-yr experiment. Modeling of the results indicates that the kinetics of oxygen uptake may be represented by a simple steady-state rate law combining enzymatic catalysis (Monod) and a first-order rate law. Combined chemical and biological data demonstrate the coupling of organic/inorganic processes during the uptake of dissolved oxygen and the progressive return to reducing conditions. Timescales for these stages are discussed. Experimental results also suggest that iron-reducing bacteria, which are robust and well-adapted microorganisms, play a key role in these interfacial processes. These results show that an operational definition of the "redox buffering capacity" in a granitic medium cannot ignore the effect of bacteria and therefore the controls on bacterial substrates (organic carbon, H_2, CH_4, CO_2). *Copyright © 2002 Elsevier Science Inc.*

1. INTRODUCTION

Granite is a potential host rock for the deep disposal of radioactive waste. A waste disposal site could be envisaged at a depth of several hundred meters in such a rock formation (Chapman et al., 1987; SKB, 1995). The time period during which the repository would be built and then filled with radioactive waste could range up to ~50 yr. Groundwater sampled in a deep granite formation, in well-controlled conditions, is usually reducing and neutral to slightly alkaline (Wikberg, 1985; Nordstrom et al., 1989; Bottomley et al., 1990; Grimaud et al., 1990; Alaux-Negrel, 1991; Grenthe et al., 1992; Laaksoharju et al., 1999). At the opening of galleries, the intrusion of oxygen perturbs mineral-solution equilibria and induces modifications in bacterial communities. The groundwater flow regime can also be strongly affected by the excavation (Mahara et al., 2001). After several years in aerated conditions (intrusion of oxygen and CO_2, active aerobic microbes), retention properties along fractures intersecting the tunnels could be significantly modified. After disposal closure, it is expected that physicochemical conditions prevailing before site opening will progressively be restored; however, the timescale and successive stages of this return to reducing conditions are poorly known. The fate and effect of dissolved oxygen (DO) have been the subject of previous investigations, especially in environments displaying redox boundaries such as lakes (De Vitre et al., 1993; Fürrer and Wehrli, 1996), the water–sediment interface (Wang and Van Cappellen, 1996) and in relation to the leaching of mine tailings (Strömberg and Banwart, 1994) or uranium ores (Adler, 1974; Cross et al., 1991). Deep granite

environments perturbed by the intrusion of aerated waters or put directly in contact with oxygen have also been examined within the context of geological waste storage. Banwart et al. (1994) studied hydrochemical perturbations during tunnel construction at the Äspö Hard Rock Laboratory. They indirectly observed that waters reaching the tunnel at a depth of 70 m remained persistently anoxic in spite of a large input of aerated shallow water at the head of a fracture zone. However, O_2 was not directly measured. These authors proposed that the oxidation of organic matter present in the first meters of fractured rock by microbial respiration processes is the major cause of this rapid oxygen uptake. They also stressed the probable role of the Fe and Mn redox systems in the persistence of anoxic conditions—for example, through the alteration of Fe(II)-bearing minerals such as chlorite.

By combining measurements of Eh potential, DO, and U concentrations, Gascoyne (1997) studied the redox evolution of groundwater at the Underground Research Laboratory of the Atomic Energy of Canada Limited in Manitoba, an experimental field site situated in a granite batholite, where boreholes permit groundwater sampling from recharge and discharge fractures. Consistent with Grenthe et al. (1992) and Banwart et al. (1994), the roles of organic matter and the Fe(II)/Fe(III) couple were apparent in this study, as evidenced by the rapid uptake of O_2 in a closed borehole section. Gascoyne (1997) also demonstrated, by use of U concentrations as a redox tracer in groundwater, that the redox perturbations along strong recharge features may reach depths greater than 400 m.

The concept of reducing capacity may be used to quantify the maximum oxidizing perturbation that can be buffered by aquatic or water–rock systems (Buffle and Stumm, 1994). However, measurements of this quantity have often been performed at conditions that are not representative of actual repository conditions (Pirhonen and Pitkänen, 1991; Turpault and

---

* Author to whom correspondence should be addressed (laurent.trotignon@cea.fr).

† *Present address:* CETE Lyon, LRPC/Environnement, 25, av. F. Mitterand, Case n° 1 F-69674 Bron Cedex, France.

Trotignon, 1992). In addition, redox buffer capacity is difficult to quantify in an open system (Rosing, 1993), where reactions between species may be strongly limited by transport processes or reaction rates. A substantial inventory of solid-state reducers (e.g., iron(II) in sulfides, silicates) is typical for many types of crystalline rocks, suggesting a large inherent O_2 reduction capacity. However, the nature and duration of the relevant processes contributing to O_2 reduction are not easily quantified.

Laboratory investigations on subsystems involving the reaction of reducing agents of interest may be used to predict in situ O_2 uptake rates or the form of kinetic rate laws. For example, laboratory studies of the iron or sulfur redox systems result in high O_2 uptake rates (Stumm and Lee, 1961; Millero, 1985; Millero et al., 1987a,b), in agreement with field observations (Gascoyne, 1997). These redox processes are also catalyzed by mineral surfaces (Tamura et al., 1976, 1980; Davies and Morgan, 1989). However, granitic groundwaters have low concentrations of reduced iron or sulfur. This observation raises the possibility of either renewal of reduced species in solution by dissolution of iron(II)- or sulfur(II)-bearing minerals; or a direct surface reaction between aqueous O_2 and specific mineral sites (White and Yee, 1985; White and Peterson, 1996). Oxygen uptake rates predicted from the major solid-state iron(II) sources in granite—that is, chlorite or biotite dissolution (Malmström et al., 1996)—are, however, low compared with field evidence. A similar prediction can be made for pyrite (Williamson and Rimstidt, 1994), as a result of its scarcity in the rock. Wersin et al. (1994) developed a simplified model of oxygen uptake in clay backfill on the basis of pyrite oxidation and determined that the timescale of oxygen uptake in this medium ranged between 7 and 290 yr; the main uncertainty was the available pyrite reactive surface area.

On the other hand, microbial processes may lead to direct uptake of oxygen (aerobic respiration) or dissolution of minerals containing reduced species (Fe(II), Mn(II), S(-II)) that will then react with DO (Lovley and Chapelle, 1995; Pedersen, 1996, 1997; Banfield and Nealson, 1997). This hypothesis raises the question of the availability and renewal of microbial substrates such as organic carbon, H_2 or CH_4 in the deep granitic medium.

To improve our knowledge of the processes and reaction rates involved when DO is introduced in a deep crystalline rock, Andra (Agence Nationale pour la Gestion des Déchets Radioactifs, France), SKB (Svensk Kärnbränslehantering AB, Sweden), and JNC (Japan Nuclear Cycle Development Institute) proposed a project (Redox Experiment, or REX) with the following two main tasks (Puigdomenech et al., 1999):

(1) In situ experiment in the Äspö Hard Rock Laboratory (HRL, Sweden; Royal Institute of Technology, Geosigma; Puigdomenech et al., 2001). A fracture section, intersected by a large-diameter borehole cored from a niche in the Äspö tunnel (−380 m under sea level), was isolated in an experimental chamber in which DO was injected and monitored together with other physicochemical parameters and microbiological evolutions.

(2) Laboratory investigations including studies of the contribution of microorganisms sampled in situ on DO uptake (Göteborg University; Kotelnikova and Pedersen, 1999a), studies of DO uptake by fracture minerals sampled in Äspö

Fig. 1. Photograph of the fracture surface on the diorite core sampled in borehole KA2861A in the HRL at Äspö (diameter, 176 mm).

(Bradford and Sheffield Universities, Terralogica), study of the interactions between minerals (Äspö diorite) and sulfate-reducing or iron-reducing bacteria (British Geological Survey) and the construction of a replica of the REX in situ experiment (CEA Cadarache and Centre National de la Recherche Scientifique).

This article presents the results obtained on the replica experiment. This experiment, performed on the core section extracted from the REX borehole, had two main objectives: first, to evaluate the usefulness of a replica approach for borehole geochemical studies; and second, to obtain experimental data that could contribute to quantifying the major processes involved during the evolution from oxidizing to reducing conditions.

2. MATERIAL AND METHODS

2.1. Sampling and Characterization of the Diorite Core

The location of the REX experimental site at the Äspö underground laboratory was selected on the basis of several criteria (Winberg et al., 1996; Puigdomenech et al., 1998, 1999): (1) minimal interference with surface and other experiments in the HRL, (2) low water flux, and (3) water chemistry corresponding to deep and confined conditions. The diorite core (176 mm in diameter) was drilled in Äspö on October 28, 1996 (borehole KA2861A). The terminal section of the core (~0.3 m in length), adjacent to the target fracture, was sawed and confined under a nitrogen atmosphere in an especially designed container. The fracture surface (Fig. 1) did not present clear signs of recent alteration or water circulation. The measurements made during and after drilling showed low water production in borehole KA2861A (Puigdomenech et al., 1999). Thin fractures parallel to the target section with a gray-white filling could be visually observed. The core was sectioned with a diamond saw into three parts:

(1) A basal section (30 mm thick) to study mineralogy and to measure the DO uptake by small diorite fragments.

(2) An intermediate section (100 mm thick), called the "ghost core," in order to simulate the real core in initial tests of the apparatus.

(3) The top section of the core (~120 mm thick), which contained the target section. This section was immediately restored in a dry nitrogen atmosphere.

Chemical analysis of a basal fragment of the core confirmed that the rock was a diorite, with a composition close to the mean composition of Äspö diorite given by Tullborg (1995). The main mineral phases of

the core were plagioclase (largely altered), K-feldspars, quartz, and chlorite; some muscovite, amphibole, and calcite were also found in the rock matrix. Sparse aggregates of magnetite, pyrite, and chalcopyrite were also identified via optical microscopy. Fracture fillings were mainly composed of epidote (pistachite type), chlorite, quartz, K-feldspar, prehnite, fluorite, and zeolite. Note that biotite, previously described by Tullborg (1995), seemed to be absent from this zone of the Äspö site and was probably totally altered and replaced by secondary products. Chlorite was widely abundant, with two habits: large crystals (>100 μm size), and a microcrystalline form (~10 μm in size). These investigations showed that the major iron(II)-bearing mineral phase present in this diorite sample should be chlorite (Fe(II)/Fe(tot) = 0.8; Tullborg, 1995). Magnetite and sulfides (pyrite, chalcopyrite) occurred in much smaller amounts.

Observation of the target section with a binocular microscope showed that the fracture surface was rough, with numerous open mineral joints and microcavities. Small mineral fragments (size <50 μm) were also found on the surface. The effective surface area of the core section was thus significantly larger than the macroscopic area deduced from simple geometric considerations. These cavities and pores could create favorable conditions for microenvironments and diffusion of oxygen into the rock matrix through the open and connected porosity could be significant. Thin fractures (<1 mm in thickness) filled with white alteration products (prehnite, calcite, clays) intersected the core throughout. Large fracture features (>1 cm in width) filled with epidote also crossed the core section. To minimize bias between the replica and in situ experiments, the fracture surface was not sterilized or treated in any way except that it was stored under a dry nitrogen atmosphere before use.

2.2. Sampling and Characterizing Groundwater

The water sampled from borehole KA2861A was saline (>300 mmol L^{-1}) with low carbonate alkalinity (~ 2 mmol L^{-1}, corresponding to a CO$_2$ partial pressure of ~10^{-4} bar). These characteristics, typical of deep crystalline bedrock (Grimaud et al., 1990; Laaksoharju et al., 1999), showed that this part of the tunnel was not perturbed by surface groundwater. Because of the low flow of water in borehole KA2861A, the groundwater used for the experiment was collected from the borehole KA2862A, 1 m distant. The deep section (15 to 16 m) of this second borehole delivered water of high salinity with low bacterial contamination at a flow rate of 2 L mn^{-1} (Puigdomenech et al., 1999). To minimize changes in water chemistry between sampling on site and utilization in the replica experiment, water was collected in Teflon-coated stainless steel bottles at the in situ pressure (~30 bar). These bottles were sterilized in an autoclave before filling and kept in a refrigerator at 5°C before use.

The speciation of the sampled groundwater was evaluated with the geochemical modeling tool CHESS 2.4 (Van der Lee, 1998). This groundwater was close to solubility equilibrium with calcite, chalcedony, gypsum, albite, illite, kaolinite, and laumontite. The in situ Eh potential was not measured but was estimated to be in the range −0.10 to −0.15 V, following the work of Grenthe et al. (1992), who showed that an equilibrium between goethite and solution is often representative of Eh field measurements in such deep granitic groundwaters.

2.3. Experimental Setup

2.3.1. Principles

One of the challenges of the experimental protocol was to reduce oxygen consumption by all components that contacted the core or the water. Preliminary experiments demonstrated that polyethyleneterephthalate (PETP) was superior to stainless steel type 316L for this purpose. Consequently, PETP was selected for the replica experiment, and stainless steel parts were eliminated to the extent possible. A schematic of the experimental setup is given in Figure 2. The target section of the core was confined in an airtight vessel (core unit), in contact with groundwater. The water was circulated by a gear pump (Ismatec, stainless steel head) through a measurement unit where Eh, pH, and dissolved O$_2$ were continuously monitored. Sampling and injection ports were also located on the circulation loop, to inject definite volumes of groundwater equilibrated with various partial pres-
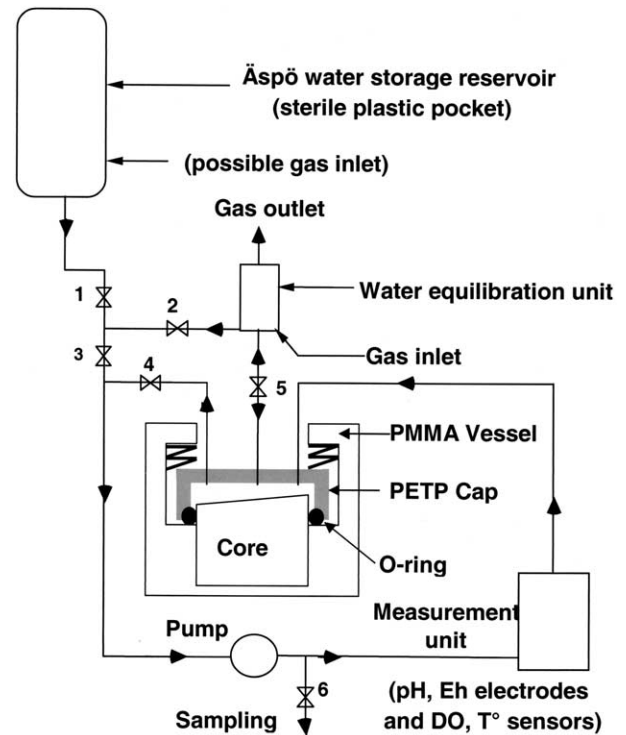

Fig. 2. Schematic representation of the setup. Main units are the core unit, where the diorite core is confined; the measurement unit, where sensors are located; and the water equilibration unit, where oxygen may be bubbled. The pumping flow rate is set at 120 mL min^{-1}. Homogenization of the water contained in the system takes ~20 min after the injection of a tracer pulse.

sures of oxygen. The working pressure was 1 bar, and the apparatus was contained in an incubator thermostated at 15°C. The core was placed in a methyl polymetacrylate vessel with an O-ring (Nitril) fitted around the core and a cap made of PETP with edges pressing the O-ring against the core (Fig. 2). The fittings, tubes, and valves were made of PEEK. Tests performed on the ghost core showed that water placed on top of the core could slowly permeate through it by following the thin fractures filled with white alteration products. Consequently, the cylindrical surface and base of the core were covered with a resin (Struers Epofix 40200029). Further leakage was minimal. Before water injection by gravity from the storage reservoir, the tubes and modules were flushed with a N$_2$-CO$_2$ (150 ppm)-H$_2$ (0.4%)-CH$_4$ (1.5%) gas mixture to obtain a low residual oxygen concentration and to mimic mean gas concentrations observed in the field. In normal operation, water circulated in a closed loop through the core and measurement units at a constant flow rate of 120 mL min^{-1} as controlled by the pump (total volume of fluid was 1178 ± 25 mL). The water equilibration unit was used to equilibrate Äspö ground water with a gas mixture containing a known concentration of oxygen. Gas mixtures used for water equilibration were usually N$_2$-CO$_2$-O$_2$ mixtures with various concentrations of O$_2$ (0 to 20%). Before the start of the experiment, the different components of the apparatus (except the core) were carefully cleaned with ethanol and then rinsed with deionized water.

2.3.2. Continuous Measurements: DO, pH, and Eh

The DO sensor (Orbisphere Moca 3600) was a polarographic cell isolated from the solution by a fluoropolymer membrane through which DO diffused and was electrochemically reduced. The current produced by this reaction was proportional to the oxygen concentration near the sensor. The contribution of the sensor to O$_2$ uptake took the form of a rate law that was first order in O$_2$ concentration, with the rate constant being close to 0.002 d^{-1}. The detection limit for the oxygen sensor was

Table 1. Chronology of the REPLICA experiment.

Date	Time (d)	Note	Pulse reference	Sample reference	Chemistry	Biology
10/06/98	0	Start		REX B1	Yes	Yes
		Initial anoxic state				
02/07/98	22	First small D.O. pulse	P1	REP02	Yes	Yes
06/07/98	26	Second small D.O. pulse	P2	REP03	Yes	No
09/07/98	29	Third small D.O. pulse	P3	REP04	Yes	Yes
15/09/98	97	First medium D.O. pulse after long anoxic period	P4	REP05	Yes	Yes
23/09/98	105	Second medium D.O. pulse	P5	REP08	Yes	Yes
05/10/98	126	Third medium D.O. pulse	P6	REP09	Yes	No
26/10/98	138	First large D.O. pulse after anoxic state	P7	REP10	Yes	Yes
09/11/98	152	Second large D.O. pulse	P8	REP11	Yes	No
23/11/98	166	Third large D.O. pulse	P9	REP12	Yes	Yes
14/12/98	187	Small D.O. control pulse	P10	REP13	Yes	No
17/12/98	190	Small D.O. control pulse	P11	REP14	Yes	No
18/12/98	191	High D.O. pulse (28 mg L^{-1})	P12a		No	No
21/12/98	194	New D.O. increase from 22 to 38 mg L^{-1}	P12b		No	No
07/01/99	211	New D.O. increase from 17 to 22 mg L^{-1}	P12c	REP15	Yes	Yes
21/01/99	225	New D.O. increase from 7 to 11 mg L^{-1}	P12d	REP16	Yes	Yes
04/02/99	239	D.O. reaches 0 mg L^{-1}				
04/03/99	267	Sampling in anoxic conditions		REP17	Yes	Yes
14/04/99	308	Sampling in anoxic conditions		REP18	Yes	Yes
11/05/99	335	Sampling in anoxic conditions and stop		REP19	Yes	Yes

~ 0.01 μmol L^{-1}. Eh (platinum) and pH (glass) combined electrodes were Xerolithe gel sensors (Mettler-Ingold) with an Ag-AgCl reference electrode in 3 mol/L KCl (reference potential at 15°C was computed to be $+213$ mV with respect to the standard hydrogen electrode, or SHE). The pH electrode was calibrated at the temperature of the experiment with commercial buffers (Schott). The Eh and pH measurements during and after oxygen pulse injections were highly reproducible, even after long operating periods. Periodically, the pH electrode was recalibrated, which revealed a slow drift of the measurements (~ 0.1 pH units over several months). Eh and pH measurements were sampled by a computer through an AD converter (National Instruments) at from 5 to 60 samples per hour.

2.3.3. Experimental Protocol

The protocol for the injection of DO pulses was based on injecting DO pulses of increasing intensity to start with small perturbations and to explore the dependency of DO uptake on initial DO concentration. At each stage, reproducibility was checked by injection of several pulses of identical intensity. Return from oxic to reducing conditions was monitored during rest periods between each series of pulses. Solution was sampled just before the injection of each pulse. A final period of high oxygen concentration was used to evaluate if the total redox buffer capacity of the system could be reached. It is important to note that the solution was only partially renewed with each pulse injection (~ 100 mL). For the final highly oxygenated period, the entire solution volume was circulated through the equilibration unit that was flushed with O_2. This protocol, described in Puigdomenech et al. (1998), was followed for the present experiment with some adaptations (Table 1). The time lag between the first series of pulses and the second one was extended to 2 months to explore the evolution toward reducing conditions. Two small DO pulses (P10, P11; 30 μmol L^{-1}) were added in order to check the effect of pump flow rate and to evaluate the influence of the evolution of microbial populations on DO uptake since the injection of pulse P1. High DO concentration (P12) was maintained for several weeks by successive injection of elevated oxygen concentrations. After the DO concentration returned to 0, the system was left isolated for 15 weeks with continuous monitoring of pH and Eh as well as periodic withdrawal of solution samples.

2.4. Chemical and Microbial Investigations

2.4.1. Solution Analyses

Major anions (Cl^-, SO_4^{2-}) were analyzed by capillary electrophoresis (Waters CIA) on 0.25-μm filtered aliquots. The elements Ca, Na, K,

Mg, Fe, and Al were determined by atomic absorption spectroscopy (Hitachi Z8200) of filtered (0.25 μm) and acidified (Suprapur HNO_3) aliquots. The elements Si, Mn, and Sr were determined by inductively coupled plasma spectroscopy (Jobin-Yvon JY38) on filtered (0.25 μm) and acidified aliquots. Samples for the analysis of total organic carbon (TOC) and inorganic carbon were collected in glass tubes that were previously calcined at 500°C for 12 h. The measurements were performed on filtered (0.25 μm) or unfiltered splits on a Shimadzu 5050A TOC meter (infrared detection). Samples were kept in a freezer before measurements. For HS^-, Fe, and Mn, some measurements or duplicate determinations were made immediately after sampling by UV absorptiometry (Merck SQ118). Cells with optical path lengths of 10 and 50 mm were used. For Mn (Merck, Spectroquant 14770), detection of a complex with formaldoxime was performed at 445 nm. For Fe (Merck, Spectroquant 14549), detection of a colored complex with [(pyridyl-2)-3-triazine-1,2,4-diyl-5,6]-4,4'-dibenzenesulfonic acid was performed at 565 nm. For HS^- (Merck, Spectroquant 14779), a reaction with N,N'-dimethyl-1,4-phenylene-diamine dihydrochloride produced the colorless leucomethylene blue, which was then oxidized to methylene blue (and colored) by iron(III). Absorption measurements were performed at 665 nm. The detection limit for HS^- was 10 μg L^{-1}.

Carboxylic ligands (formate, acetate, propionate, phthalate, oxalate, citrate) were determined by ion chromatography (Dionex 4000i, AS11 column, NaOH eluent, gradient mode). The detection limit was ~ 1 mg L^{-1} for all these compounds. Dissolved organics were also characterized by gas chromatography on a capillary column (HP InnoWax 19091N-133) coupled to mass spectroscopy (Hewlett-Packard). Two injection techniques were used: direct injection of a 1-μL sample (100-fold dilution), and solid-phase microextraction with a polyacrylate fiber of a sample diluted 10-fold.

2.4.2. Microbial Investigations

The culture protocols are summarized in Table 2. Liquid samples collected at the sample port were drawn off in a sterile syringe and immediately placed in sterile vials. The vials were immediately sent to the microbiology laboratory in a refrigerated package, and the culture media were seeded within 24 h. For biofilm characterization at the end of the experiment, a synthetic sterile cotton wool piece was rubbed against a 2 to 6 cm^2 square section of core surface. The sterile cotton wool was then immediately placed in a neutral suspension (deaerated, with culture salts but without specific substrates). The vial containing the cotton wool was then shaken and ultrasonicated for 5 min to remove the biofilm from the cotton wool. The seeding of culture media was then performed with 1 mL of this suspension. Sampling of biofilm is

Table 2. Analytical protocols for microbiological determinations.

Bacteria	Culture medium or method	Concentration determination
Sulfate reducers	TK Labège anaerobic + lactate and acetate	After 3 weeks, blackening by Fe sulfide
Aerobes	Organic rich aerated	After 1 week, solution blur
Fermentative anaerobes	Organic rich deaerated	After 2 weeks, yellowing of pH color indicator
Methanogens	Anaerobic medium (H_2 20%/CO_2 80% + acetate and formiate)	After 5 weeks GC detection of CH_4
Methanotrophs	Specific aerobic medium + (5% CH_4 in the gas phase, acetate + formiate)	After 5 weeks, GC detection of CH_4
Iron reducers	Specific aerobic medium	After 5 weeks, determination of iron(II) by colorimetry
Total microbes[a]	Suspension put in contact with 4'6-diamino-2 phenylindole DAPI and fixed on a 0.2-μm filter treated with Irgalan black	Detection of DAPI fluorescence by cells under the microscope

[a] DAPI = 4'6-diamino-2 phenylindole.

difficult, especially on rough surfaces, and generally has a low yield, leading to an underestimation of attached bacterial populations (Allen et al., 1980). Nevertheless, a comparison between different surface samples is possible. The types of bacteria listed in Table 2 were thought to be the most active during perturbation by DO. Other types of bacteria, such as H_2 oxidizers and Fe(II) oxidizers, were not quantified during the experiment, although they were detected at Äspö (Pedersen, 1997; Kotelnikova and Pedersen, 1999a).

2.4.3. Investigations on the Solid Phase

Several investigations were performed on the rock before the experiment. Petrographic thin sections were made from a basal section of the core and examined with an optical microscope or a scanning electron microscope (SEM) (Philips XL30) coupled to an energy dispersive X-ray spectrometer (Oxford-Link). The initial surface of the core was also studied under a binocular microscope. The bulk rock was characterized by classical wet chemical analyses and X-ray diffraction techniques performed on powders. After the experiment, fragments were collected at the core surface and examined with the binocular microscope and SEM. An attempt was made to perform observations before and after the experiment on selected areas.

2.5. Data Processing and Modeling

Analytical concentration data obtained on sampled solutions were processed with the geochemical modeling tools CHESS 2.4 (Van der Lee, 1998) and the GWB (Geochemists Workbench; Bethke, 1994). Preliminary processing of DO uptake kinetics was performed with Microsoft Excel. A computer program for kinetics modeling was written in Fortran 77 using the SLATEC numerical libraries (DDEABM, DNSQE) and was run on a SGI-IRIX6.5 work station.

3. RESULTS

3.1. Results Obtained during the Setup Tests

Tests conducted in small PETP vessels showed increasing O_2 uptake rates in repetitive blank runs without any change in experimental conditions. By adding increasing concentrations of microbial inhibitors (first NaN_3, then formaldehyde), this effect was shown to originate from microbial oxygen consumption. Tests, described elsewhere in detail (Puigdomenech et al., 1998), were then continued with the ghost core. Results of microbial investigations showed a development of both aerobic and sulfate-reducing bacteria (SRB). This meant that some of these bacteria (i.e., SRB) originated from the Äspö site, either from the water or the rock. These bacteria survived DO pulses and then recolonized the experimental setup. Microbial studies were then added to the protocol. A long experiment was then conducted on the ghost core to ensure that the apparatus would

operate correctly over time periods of at least 2 months. Reducing conditions (Eh(SHE) = −150 mV for pH = 6.8) were obtained after ~5 weeks in anoxic conditions.

3.2. Replica Experiment: DO Uptake Kinetics

Oxygen concentrations decreased more linearly at lower (<30 μmol L^{-1}; Fig. 3a) rather than at higher initial concentrations (200 to 300 μmol L^{-1}, Fig. 3b). Noisy signals in pulses P4 and P8 were caused by silver deposition on the internal face of the sensor membrane. Mean O_2 uptake rates increased over pulses P1 to P3 and decreased over pulses P4 to P9. Still, the
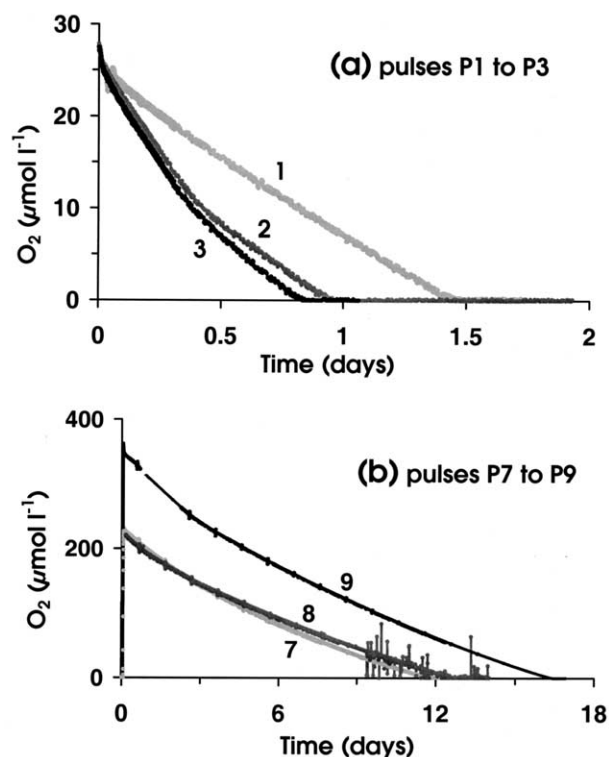
Fig. 3. Evolution with time of dissolved O_2 concentration during (a) pulses P1 to P3 (1, 2, 3), (b) pulses P7 to P9 (7, 8, 9). Kinetic study of pulses P2 and P3 indicated that possibly two successive Monod processes were active during O_2 uptake. Noise during P8 was due to deposits on the O_2 sensor membrane that was changed before P9.
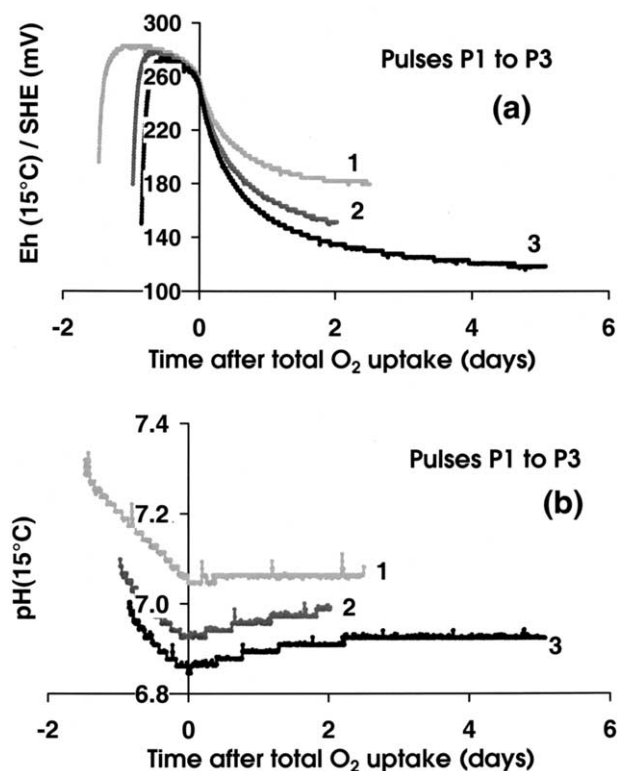
Fig. 4. Evolutions with time of (a) Eh (scaled to normal hydrogen reference) and (b) pH during pulses P1 to P3 (1, 2, 3). The timescale origin has been shifted to the moment when O_2 is totally depleted in the solution. At this moment, pH decrease stops and a sudden drop in Eh is observed. A similar evolution is observed for all pulses.

Fig. 5. Representation in Eh-pH diagrams of the trajectories followed by data points from the beginning of an O_2 pulse (arrow) to reducing conditions at 15°C. (a) Testing of the setup with the ghost core. At O_2 injection, Eh increases at constant pH; pH then decreases at nearly constant Eh, due to bacterial respiration. Eh then decreases (O_2 totally depleted) and reaches the magnetite-solution boundary (A). The data points follow this boundary when Eh suddenly decreases for pH $\sim$6.4 (B) and reach a region close to the pyrite–solution boundary (C). The vertical dotted line represents the predominance zones for H_2CO_3 (below pH 6.4) and HCO_3^- (above pH 6.4). (b) Period from the beginning of pulse 3 (arrow) to reducing conditions. In this case, equilibrium with goethite is proposed to explain the evolution of data points. The diagrams were computed by GWB (Bethke, 1994).

mean rate of DO uptake was 10 to 30 μmol O_2 L^{-1} d^{-1}. At the beginning of all pulses, a transient period of several hours up to 2 d was observed, during which time oxygen uptake rates decreased rapidly. Other oxygen pulses performed after P9 showed similar characteristics.

3.3. Evolution of pH and Eh during O_2 Pulses

Evolutions of pH and Eh during the injection of O_2 pulses followed reproducible trends (Fig. 4). A systematic pH decrease was observed in the period when O_2 was consumed, and then pH increased slowly at the beginning of the anoxic period. The successive injection of oxygen pulses in the setup thus led to a progressive acidification of the solution. When oxygen was present, the measured potential was stable ($+270$ to $+300$ mV/SHE) and independent of O_2 concentration. When O_2 was consumed, a rapid decrease of the potential was observed, with values reaching about $+100$ mV/SHE in 1 week, with a slow continual decrease thereafter.

3.4. Evolution of pH and Eh during Long Anoxic Periods

During several periods, no oxygen pulses were injected and the setup was totally isolated. The first of these periods (50 d) was monitored during the test of the setup with the ghost core (see section 3.1). By use of GWB (Bethke, 1994), measured pH and Eh values were plotted on a Eh-pH diagram (Fig. 5a).
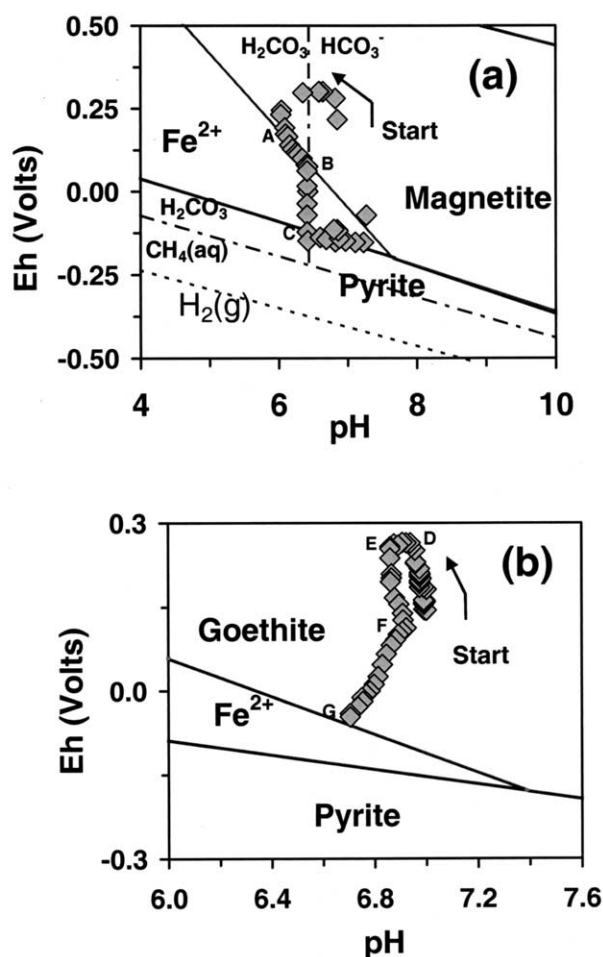
Phase limits were computed taking into account analyses of the solution performed at the end of the anoxic period. At the beginning of the reaction path (pH $\sim$7 and Eh $\sim$+0.2 V), oxygen was introduced and the Eh rapidly increased (start arrow on Fig. 5a). Then during O_2 uptake, pH decreased while Eh remained constant until anoxic conditions were reached. Eh then rapidly dropped and reached an apparent equilibrium between magnetite and solution (point A on Fig. 5a). Data points followed this limit until pH reached $\sim$6.4 (point B on Fig. 5a). Eh then suddenly dropped and the data points plotted close to the pyrite solution limit (point C on Fig. 5a).

Another anoxic period ($\sim$60 d) was studied between pulses P3 and P4 (Figs. 5b and 6). After the Eh increase and pH drop linked to oxygen uptake (start arrow to points D and E on Figs.
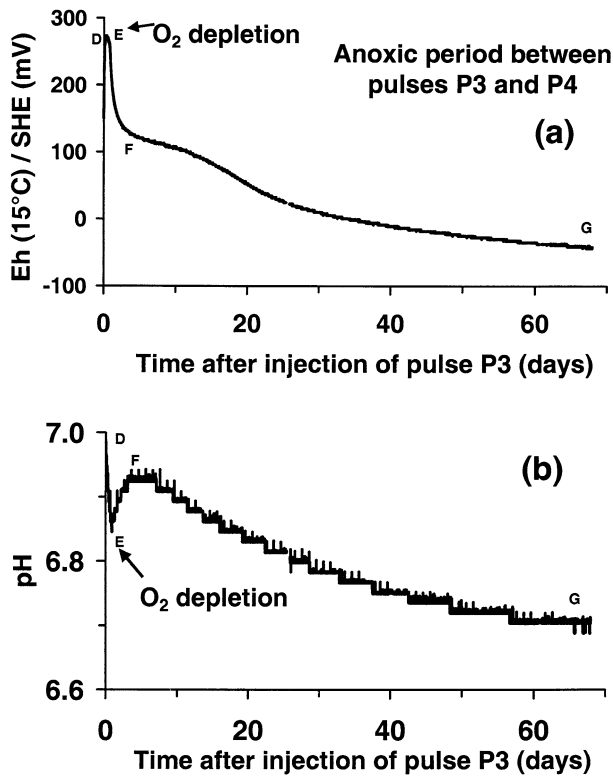
Fig. 6. Evolution of (a) Eh and (b) pH vs. time for the period from the beginning of pulse P3 to reducing conditions. These curves display along the time parameter the Eh-pH data points shown in Fig. 6b. The initial pH drop is clearly linked to aerobic respiration because it stops at total oxygen depletion.

5b and 6), Eh decreased rapidly when oxygen disappeared (from E to F on Figs. 5b and 6) and then decreased continuously (from F to G). The representative data in the Eh-pH diagram followed from F to G a direction nearly perpendicular to the goethite solution limit and finally reached this limit (the computed limit on the diagram correspond to Fe concentrations at the end of the run). The final anoxic period (after pulse P12) was also represented on an Eh-pH diagram (not shown) and it was found that the data also accumulated on the goethite solution equilibrium limit. The major results of the investigations on the evolution of the setup in anoxic conditions are thus the following: (1) the return to reducing conditions took at least 8 weeks after oxygen had been depleted; (2) the measured values of pH, Eh and solution concentrations were consistent with equilibria involving iron containing minerals; and (3) the reaction path was not always the same in the different instances. Eh-pH diagrams were also constructed by means of Mn concentration data and Mn containing minerals (oxyhydroxides, carbonates) but no correlation was observed with the experimental Eh-pH data.

3.5. Chemistry of Solutions

Solution analytical data are given in Table 3 and major trends are reported in Figure 7. The concentrations of major elements (Na, Ca, Cl, Mg) were stable. Potassium concen-

trations increased strongly with time, probably as a result of the release of KCl filling solution from the combined Eh and pH electrodes. Silicon concentrations were stable (solution was close to saturation with chalcedony) but increased slightly during anoxic periods. Manganese concentrations were close to 5 μmol L^{-1} except during anoxic periods, when they increased sharply and exceeded 20 μmol L^{-1} after several weeks. Dissolved iron concentrations followed similar trends. The first samples had low concentrations ($\sim$0.4 μmol L^{-1}), and just before P4 (end of the anoxic period) they reached 10 μmol L^{-1}. During pulses P4 to P12, iron concentrations stabilized around 2 μmol L^{-1}. A greater increase up to 18 μmol L^{-1} was observed during the last anoxic period (Fig. 7b). The rate of increase of dissolved iron is roughly the same for the two anoxic periods. Aluminium concentrations fluctuated with no clear trend. TOC concentrations in solution increased greatly, up to more than 40 mmol L^{-1} (Fig. 7d). More detailed characterizations of this organic carbon were also performed. This included the measurement of simple dissolved organic ligands and a qualitative identification of larger molecules by gas chromatography techniques. Simple carboxylates concentrations were always low (Table 3). Qualitative gas chromatography runs enabled us to identify the following major molecules: ethanol 2,2'-oxybis (=diethylene glycol), morpholine, dibutylphthalate, bis(2-ethylhexyl) phthalate, nonanal $C_9H_{18}O$, and decanal $C_{10}H_{20}O$. Among these compounds, those containing phthalate can clearly be related to a release by the PETP cap and the epoxy resin used to seal the cylindrical part of the core. The inorganic carbon concentration (Fig. 7c) also markedly increased with time, in agreement with the progressive acidification of the solution. The computed CO_2 partial pressure also increased and stabilized at the end of the experiment (to $\sim$0.015 atm). Sulfate concentrations were relatively stable with a tendency to decrease (Fig. 7e). The different data sets were examined with the geochemical speciation tool CHESS 2.4 (Van der Lee, 1998) to evaluate the temporal evolution of representative mineral saturation indexes (Fig. 8). The calcite saturation index became strongly negative after the injection of the first oxygen pulses then increased even though additional pulses were injected (Fig. 8a). The injection of the large pulse P12 resulted in the calcite saturation index again becoming negative and the return to equilibrium was incomplete even after 5 months. Silicate mineral saturation indexes were also perturbed by the injection of oxygen (Figs. 8b–d), although it was not possible to identify which phases were effectively dissolved or precipitated. Finally, the solution was near saturation with respect to gypsum throughout the experiment.

3.6. Microbial Activity

Three groups of bacteria strongly developed during the experiment: aerobes, fermentative anaerobes, and iron-reducing bacteria (IRB) (Table 4). In addition, a strong increase in SRB was observed at the end of the experiment with the onset of marked reducing conditions. Two groups of bacteria observed in the Äspö tunnel did not develop at all: methanogens and methanotrophic bacteria (Kotelnikova and Pedersen, 1999a).

Table 3. Solution analyses[a].

Sample	Date	Ca (mmol L⁻¹)	Na (mmol L⁻¹)	K (mmol L⁻¹)	Mg (mmol L⁻¹)	Al (μmol L⁻¹)	Fe (μmol L⁻¹)	Si (mmol L⁻¹)	Mn (μmol L⁻¹)	Sr (mmol L⁻¹)	Cl⁻¹ (mmol L⁻¹)
REX B1	10/06/98	126	165	0.46	1.5	1.3	0.3	0.14	4.0	1.1	436
REP02	02/07/98	104	133	5.42	1.4	2.4	0.5	0.14	4.4	1.1	458
	02/07/98						0.3				
REP03	06/07/98	139	144	4.45	1.7	<1	0.5	0.14	4.6	1.2	408
	06/07/98					<1	0.4				
REP04	09/07/98	144	155	4.40	1.6	<1	0.9	0.14	4.7	1.1	468
REP05	15/09/98	141	151	12.4	1.5	<1	6.6	0.16	5.2	1.1	473
	15/09/98						10.7		23.7		
REP08	23/09/98	137	162	13.8	1.5	<1	2.4	0.17	5.0	1.2	462
	23/09/98					2.2	0.5		0.5		
REP09	05/10/98	139	161	14.2	1.6	<1	2.9	0.18	5.2	1.3	467
REP10	26/10/98	144	162	15.3	1.5	<1	4.3	0.18	5.4	1.2	475
REM11	09/11/98	139	157	12.9	1.5	1.4	2.9	0.16	5.3	1.2	453
REP12	23/11/98	140	151	11.9	1.5	1.7	3.2	0.16	5.3	1.2	463
REP13	14/12/98	141	144	12.1	1.6	1.3	3.0	0.14	5.6	1.2	439
REP14	17/12/98	138	163	11.1	1.6	1.4	2.8	0.14	5.5	1.2	418
REP15	07/01/99	147	154	11.0	1.6	1.6	1.6	0.14	5.4	1.2	423
REP16	21/01/99	146	142	14.3	1.6	2.3	1.9	0.14	5.8	1.1	411
REP17	04/03/99	103	136	18.8	1.5	1.8	4.6	0.14	6.0	1.1	417
REP18	14/04/99	145	130	22.2	1.7	1.7	8.1	0.17	6.3	1.2	424
	14/04/99						12.5		16.9		
REP19	11/05/99	138	125	19.7	1.6	1.4	10.9	0.18	6.1	1.1	442
	11/05/99						17.9		19.7		

[a] For some samples, duplicate measurements of Fe and Mn were made using atomic absorption or UV-visible spectrometry. Uncertainty is ~5%

The absence of these types of bacteria in our experiment may have been linked to an inhibitory effect of high concentrations of organic carbon (S. Kotelnikova, personal communication) or to an insufficient activity of methane. In the initial period of the experiment (small O_2 pulses), strong increases in total microbe numbers were observed that correlated with increases in aerobes and IRB populations (Fig. 9a). Fermentative anaerobes increased strongly during the first anoxic period (between pulses 3 and 4) but showed a marked decrease when higher concentration oxygen pulses were injected (Fig. 9b). A similar decrease was observed for IRB. This correlation shows that IRB includes both microaerophilic aerobes and cells able to adapt to anaerobic conditions, which agrees with previous studies on these types of microorganisms (Nealson and Saffarini, 1994; Lovley and Chapelle, 1995; Barns and Nierzwicki-Bauer, 1997; Kotelnikova and Pedersen, 1999a). The strong increase in dissolved iron during anoxic periods is correlated to the development of IRB. Consequently, oxygen pulses seemed to trigger changes in bacterial populations. SRB evolution showed that in spite of strong oxygenation, this group was able to grow again when conditions became favorable. This suggests that reducing microenvironments persisted at the surface of the core. Results of biofilm investigations confirmed this hypothesis (Table 5) and the diorite surface was the preferred SRB location. Fermentative anaerobes were present mostly on the sealing epoxy resin; this suggests that this plastic compound could also have been one of the sources of dissolved organics detected in solution. Aerobes and IRB were present at significant levels both on plastic surfaces and on the core. Superficial cell densities were in all cases not compatible with continuous biofilm formation.

3.7. Solid Phases

At the end of the experiment, several fragments were carefully detached from the core surface. It was then possible to compare these "external surfaces" to "internal surfaces," which were in contact with water only through channels or fractures. These observations showed strong corrosion features on calcite crystals found both on the external surface (Fig. 10a) and internal surfaces. Clay phases containing Si, Al, Mg, and Fe were observed on both external and internal surfaces; on internal surfaces, they displayed sharp edges whereas rounded shapes were observed on external surfaces, which suggests dissolution reactions (Fig. 10b). Pyrite crystals showed no alteration signs at the scale of SEM observation.

4. DISCUSSION

The primary aim of this investigation was to document and quantify DO uptake in an integrated experiment simulating groundwater conditions in a fracture of a deep granitic formation. O_2 consumption was demonstrated and the pathway from oxic to reducing conditions, followed by monitoring Eh, pH, water composition, and microbial populations, was shown to extend over several weeks. A number of candidate processes causing DO uptake were listed in the introductory section. Trends in the results, especially for dissolved iron and microbial evolutions, suggested the simultaneous action of several of them. With a view to understanding more precisely which processes were responsible for these evolutions, O_2 uptake kinetic data were carefully examined. $O_2(aq)$, in opposition to other species such as H^+, was indeed the sole chemical species whose concentration variations were governed only by reac-

Table 3. (Continued).

SO4^{2-} (mmol L^{-1})	HS$^-$ (µmol L^{-1})	TOC unfiltered (mmol L^{-1})	TOC filtered (mmol L^{-1})	Inorganic C unfiltered (mmol L^{-1})	Inorganic C filtered (mmol L^{-1})	HCOO$^-$ formate (mmol L^{-1})	CH$_3$COO$^-$ acetate (mmol L^{-1})	CH$_3$CH$_2$CO$_2^-$ propionate (mmol L^{-1})	Phthalate (mmol L^{-1})	Oxalate (mmol L^{-1})	Citrate (mmol L^{-1})	pH (15°C)
8.8		0.1		0.13								
9.7		9.9				<0.02	0.02					7.65
												7.23
9.1		13.4		0.17		<0.2	0.04					
												7.08
10.0		13.3		0.18		<0.04	0.02					
9.8		32.6		0.28		<0.04	<0.03	<0.03	<0.01	<0.02	<0.01	6.99
	1.5											6.70
7.6		24.1	23.8	0.45	0.38	<0.04	<0.03	<0.03	<0.01	<0.02	<0.01	
	25.7											6.72
7.8		26.0	25.9	0.51	0.50	<0.04	<0.03	<0.03	<0.01	<0.02	<0.01	
8.1		27.9	27.6	0.62	0.69							6.69
7.3		25.4	26.6	0.94	0.92	<0.04	<0.03	<0.03				6.69
8.1		24.3	23.5	1.13	1.31							6.58
7.1		21.1	21.6	1.43	0.96	<0.04	0.07	<0.03				6.56
6.9												6.61
7.2		23.5	23.6	1.17	1.16							6.63
6.6		27.1	26.6	1.27	1.37							6.34
7.0	0.3		42.3		1.18	<0.04	0.07	<0.03				5.98
6.9		46.0										5.90
	0.3											6.00
7.7			44.4		0.95	<0.04	0.07	<0.03				
	7.6											6.06

for Ca, Na, K, Mg, Si, Sr, Cl$^-$, and SO4^{2-}, ~10% for Al, Fe, Mn, TOC, and ~20% for HS$^-$.

tions in which it was consumed. In addition, the high sampling frequency of DO concentration made possible such an analysis, which was not possible for other species, such as iron or sulfate. Specific procedures were followed for the processing of O$_2$ uptake kinetic data. First, a numerical time derivative of the O$_2$ concentration was computed and displayed as a function of the aqueous O$_2$ concentration. This representation made it possible to identify the best suited kinetic model by using guidelines suggested by a review of previous literature. The parameters of the kinetic model were then optimized by least squares regression of the O$_2$ vs. time curve. For this procedure, the kinetic model was represented by an explicit finite difference function rather than by an implicit analytical formulation, to avoid the singularities encountered in some representations of the solution. This handling of O$_2$ data showed that all DO pulses could be closely simulated by a steady-state kinetic rate law that combines first-order and Monod-type contributions (Michaelis-Menten kinetics; cf. Rittmann and VanBrisen, 1996):

$$\frac{d[O_2]}{dt} = -\frac{k_1[O_2]}{K_1 + [O_2]} - k_2[O_2], \tag{1}$$

where [O$_2$] stands for O$_2$ concentration in solution, t is time, k$_1$ (µmol L^{-1} d^{-1}) is the maximum rate for the Monod-type rate law, K$_1$ (µmol L^{-1}) is the critical concentration of the electron acceptor, and k$_2$ (d^{-1}) is the rate constant of the first-order contribution. Approximate values for these rate constant parameters are 10 to 30 µmol L^{-1} d^{-1} for k$_1$, ~0.2 µmol L^{-1} for K$_1$, and 0.03 to 0.1 d^{-1} for k$_2$. The comparison between this kinetic model and DO data is illustrated in Fig. 11 for pulse P8. The time derivative of DO (dark line, Fig. 11a) varies strongly

between 230 and 180 µmol L^{-1}; this corresponds to the first 2 d of pulse P8 (Fig. 11b). The rest of the pulse is well simulated by the kinetic rate law form given in Eqn. 1 (gray line in Figs. 11a,b). About 64 kJ of energy are required to produce 1 g of biomass ($\sim$10^9 cells) (Thauer and Morris, 1984). Taking into account the magnitude of k$_1$ and supposing that acetate oxidation is the energy yielding process, a cell production rate of 10^4 to 10^5 d^{-1} is estimated, a figure roughly compatible with measured solution and biofilm data (Tables 4 and 5). Strikingly, the kinetic constants k$_1$ and k$_2$ vary over a rather limited range during the whole experiment, even though physicochemical conditions and bacterial populations evolve upon injection of successive DO pulses. For example, the fitted value for k$_1$ in pulse P1 ($\sim$16 µmol L^{-1} d^{-1}) is larger than the fitted value for pulse P7 ($\sim$10 µmol L^{-1} d^{-1}) although aerobic bacteria in solution have increased by several orders of magnitude between these pulses (Table 4). After pulse P9 (350 µmol L^{-1}), two small control pulses P10 and P11 (30 µmol L^{-1}) gave a similar result to pulse P1: k$_1$ $\sim$ 13 µmol L^{-1} d^{-1} for both P10 and P11. In addition P11 was conducted with different flow conditions showing that solution convection was not a rate-limiting factor for oxygen uptake by aerobic respiration. Another possible explanation for the constancy of rate constant k$_1$ is that a limiting step for the respiration of DO is linked to the carbon substrate utilization or to the availability of specific substrates such as nitrogen or phosphorus (K. Pedersen, personal communication). Although organic carbon concentration increases quite a bit in solution (Fig. 7d), the concentration of preferred bacterial substrates such as acetate remains low (Table 3). This could mean that organics released by the resin or PETP cap are slow to transform into easily assimilated mole-
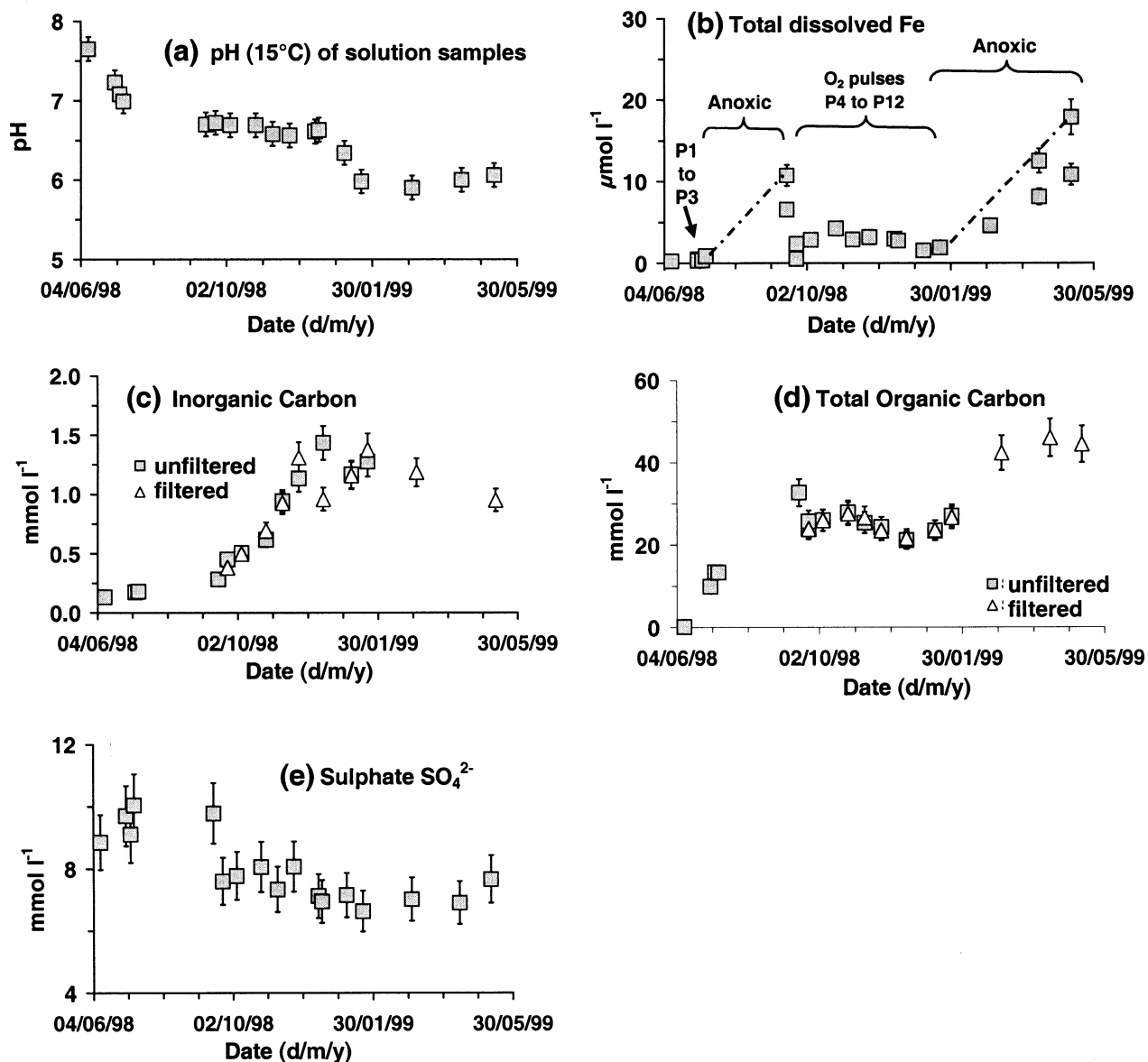
Fig. 7. Evolution of several important chemical parameters vs. time: (a) pH of sampled aliquots, (b) total dissolved iron, (c) inorganic carbon, (d) TOC, and (e) sulfate.

cules. It is therefore suggested that the constancy of the k_1 rate factor is linked to a rate-limiting factor in substrate degradation and/or to the limited availability of a specific, but undetermined, substrate. The aerobic respiration may be schematically represented by the oxidation of acetate,

$$CH_3COO^- + 2O_2 \rightarrow 2HCO_3^- + H^+. \qquad (2)$$

The initial rapid pH decrease observed when DO pulses are injected (Fig. 4b) is clearly linked to bacterial respiration and CO_2 production (Eqn. 2). Solution pH drops from 7.5 to values close to 6.0 (Fig. 7a) because the Äspö groundwater is weakly pH buffered; the stabilization of pH between 6.0 and 6.5 after several DO pulses reflects the increasing buffering effect by the HCO_3^-/H_2CO_3 system, which has a pKa = 6.4 at 15°C. Or-

ganic molecules probably also impacted the pH to some extent. The pH excursion caused by oxygen intrusion induces calcite to dissolve, as shown by the analysis of saturation indexes and by SEM investigations (Figs. 8a and 10a). This process involves large mass transfers and is certainly one of the major driving forces explaining the reversal of pH trend at the end of DO pulses (Fig. 4):

$$CaCO_3(calcite) + H^+ \leftrightarrow Ca^{2+} + HCO_3^-. \qquad (3)$$
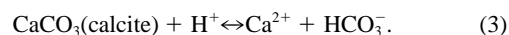
Other mineral phases, in particular silicates such as oligoclase, should also contribute to the pH increase but with slower kinetics (Stumm and Morgan, 1996). Consequently, recovery of the perturbation caused by the intrusion of O_2 involves alkalinity fluxes that are rate controlled by mineral dissolution.
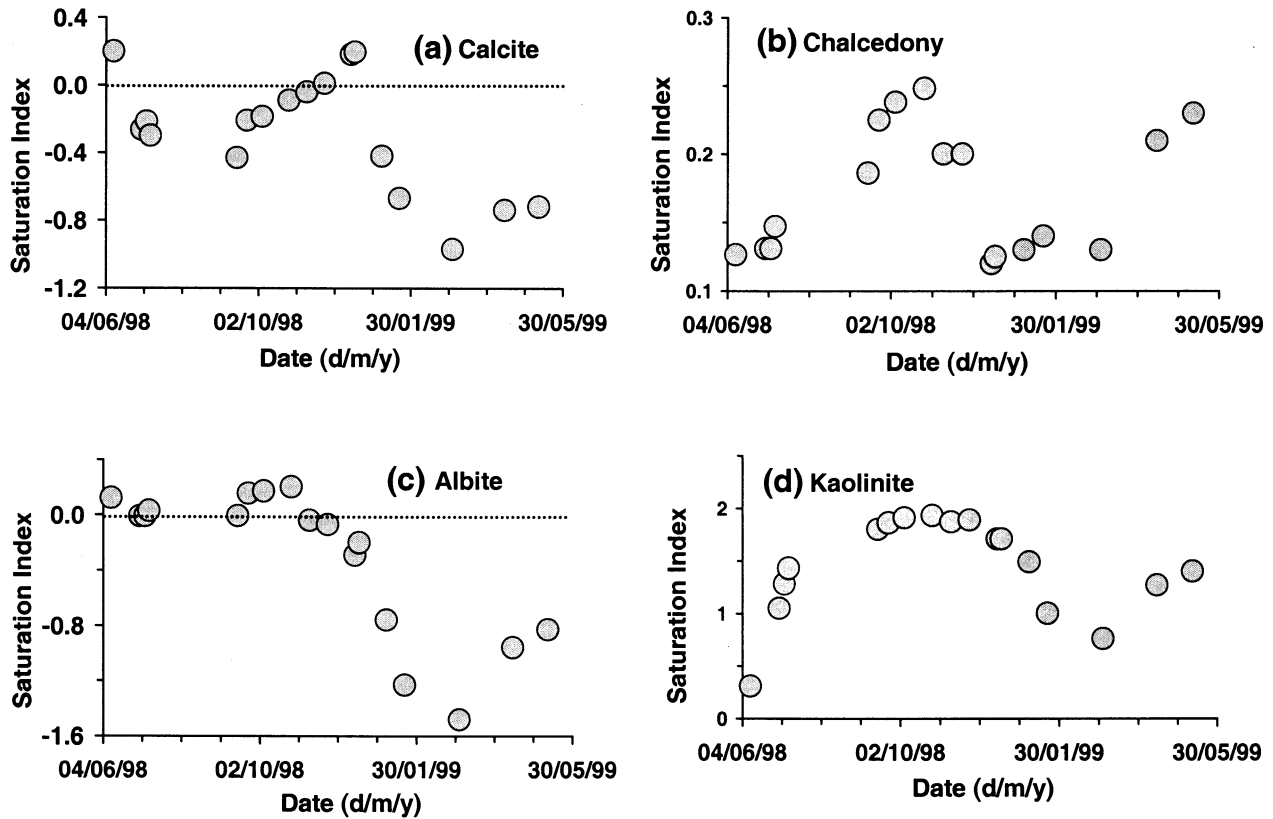
Fig. 8. Evolution of saturation indexes of the solution with respect to (a) calcite and (b) chalcedony. The saturation indexes of aluminosilicate phases could not be accurately evaluated because of high uncertainties or fluctuations in measured Al concentrations (Table 6). For these minerals, similar computations were performed with the assumption of constant Al concentration (4×10^{-9} mol $L^{-1} \sim 10^{-4}$ mg L^{-1}). This value of Al concentration was selected because it predicted equilibrium of the initial groundwater with albite, kaolinite, and laumontite. Results are shown for albite and kaolinite in (c) and (d).

The aqueous oxidation of Fe(II) by DO, described by the reaction

$$4Fe^{2+} + O_2 + 10H_2O \rightarrow 4Fe(OH)_{3aq} + 8H^+ \qquad (4)$$
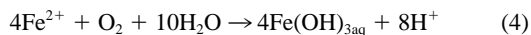
is a candidate process to explain the first-order rate term k_2 in Eqn. 1. However, the rate law found in literature for the aqueous oxidation of Fe(II) is strongly dependent on proton activity (Stumm and Lee, 1961; Tamura et al., 1976; Sung and Morgan, 1980). Wehrli (1990), assuming that the total aqueous concentration of iron(II), [Fe(II)aq], is close to the aqueous

Table 4. Microbiologic analyses of the solution samples.[a]

Sample	Date	Total microbes, log(cells mL^{-1})	heterotrophic aerobes, log(cells mL^{-1})	Fermentative anaerobes, log(cells mL^{-1})	Sulfate-reducing B log(cells mL^{-1})	Iron-reducing B log(cells mL^{-1})
REX B1	04/06/98	6.07	1.40	0.40	1.40	1.40
REP02	02/07/98	6.43	3.40	0.78	1.40	4.40
REP04	09/07/98	7.66	3.78	0.40	ND	4.78
REP05	14/09/98	7.56	4.40	1.85	ND	4.40
REP08	23/09/98	7.93	5.40	5.40	ND	5.04
REP10	26/10/98	7.42	4.85	6.40	ND	5.40
REP12	24/11/98	7.54	4.78	5.40	0.40	2.40
REP15	07/01/99	7.44	4.78	4.40	0.40	2.78
REP16	21/01/99	7.13	5.40	3.40	n.d.	3.40
REP17	04/03/99	7.05	3.70	3.78	0.40	3.78
REM18	14/04/99	7.39	4.40	2.40	2.40	6.40
REP19	11/05/99	7.61	5.04	1.85	3.40	3.78

[a] ND = not detected. Methanogen and methanotrophic bacteria were always under detection limit.
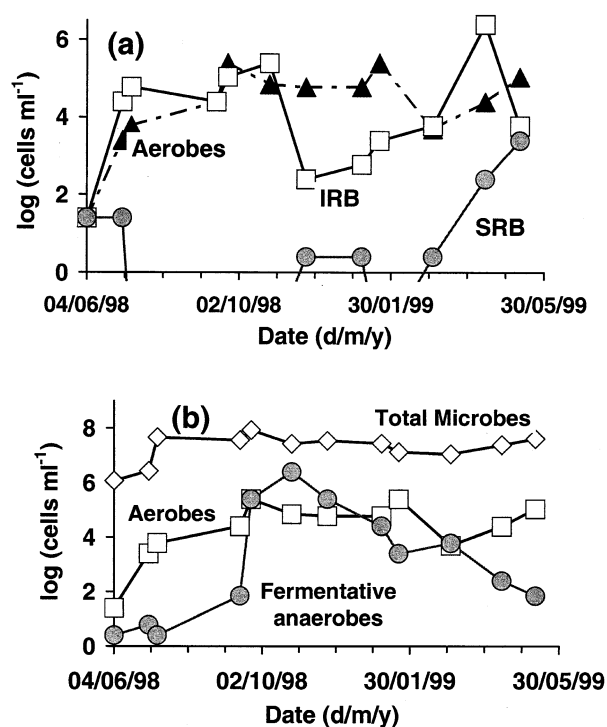
Fig. 9. Evolution of microbial populations during the replica experiment. In the initial period of the experiment, a clear correlation is observed between aerobes and IRB, suggesting that at least a part of IRB are also facultative aerobes.
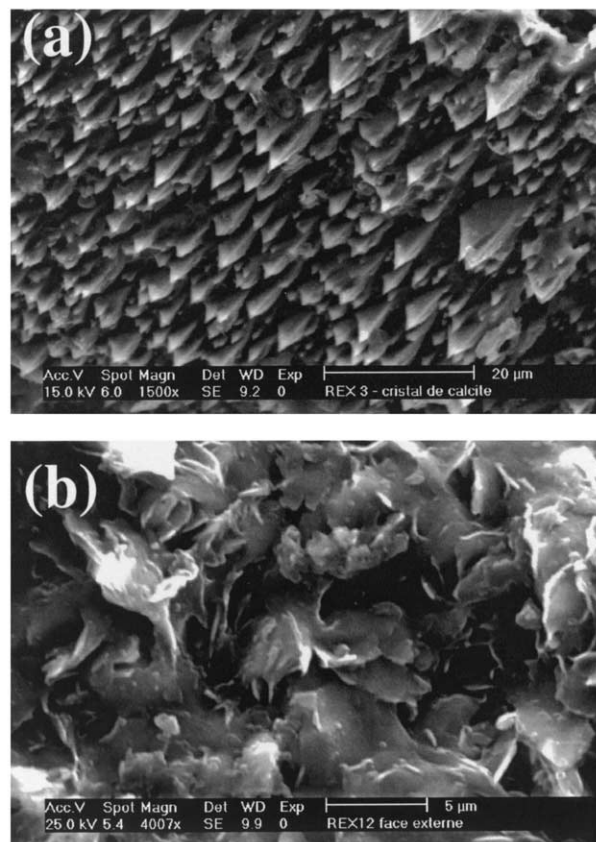
Fig. 10. SEM images of fragments of the diorite core at the end of the replica experiment. (a) Typical dissolution features observed at the surface of calcite crystals. (b) Chlorite crystals found on the face exposed to water, showing rounded edges attributed to dissolution processes.

concentration of Fe^{2+}, gives the following expression for this rate law:

$$\frac{d[Fe(II)_{aq}]}{dt} = -\left\{ k_a + \frac{k_b}{[H^+]} + \frac{k_c}{[H^+]^2} \right\} [Fe(II)_{aq}][O_2]. \quad (5)$$

In this expression, k_a, k_b, and k_c are constants. Over the pH range of the replica experiment, the k_a and $k_b/[H^+]$ contributions are minor compared with the $k_c/[H^+]^2$ term (Wehrli, 1990). Speciation calculations showed that in our experiment, Fe^{2+} was the dominant aqueous species of Fe(II), and Eqn. 5 therefore takes the following simplified form:

$$\frac{d[Fe(II)_{aq}]}{dt} \approx \frac{d[Fe^{2+}]}{dt} = -\frac{k_c}{[H^+]^2}[Fe^{2+}][O_2]. \quad (6)$$

This is not compatible with a first-order rate constant k_2 inde-

pendent of time. However, homogeneous oxidation of Fe(II) could be linked to the initial rapid uptake observed on several curves (e.g., Figs. 3 and 11). The oxidation of aqueous Mn(II) might also contribute to the initial fast DO uptake. This process is slow in aqueous solution but may be greatly accelerated in presence of mineral surfaces (Diem and Stumm, 1984; Davies and Morgan, 1989; Junta and Hochella, 1994). Catalytic and autocatalytic reaction schemes have also been advanced for the oxidation of Fe(II) by $O_2(aq)$ in the presence of Mn(IV) and Fe(III) hydroxides (Tamura et al., 1976, 1980; Sung and Morgan, 1980; Van Cappellen and Gaillard, 1996). A complete

TABLE 5. Microbiologic analyses of surface samples collected at the end of the experiment.[a]

Sample	Surface area (cm^2)	Total microbes (cell cm^{-2})	Heterotrophic aerobes (cell cm^{-2})	Fermentative acidogenic anaerobes (cell cm^{-2})	Sulfate reducing (cell cm^{-2})	Iron reducing (cell cm^{-2})
Core 1	2	3.9×10^8	6.0×10^4	1.1×10^4	1.3×10^4	2.5×10^4
Core 2	3	1.8×10^8	1.7×10^5	1.7×10^4	1.7×10^5	1.7×10^4
Epoxy resin	5	1.4×10^7	1.0×10^3	1.0×10^5	10	1.0×10^4
PETP cap	6	6.7×10^5	1.1×10^5	1.0×10^2	10	24
O-ring	5	8.5×10^5	2.3×10^5	6.6×10^2	2	1.9×10^4

[a] As a result of the low yield of the biofilm sampling technique, bacterial surficial densities are probably underestimated by a factor between 1 and 10. Comparison between samples is nevertheless possible.
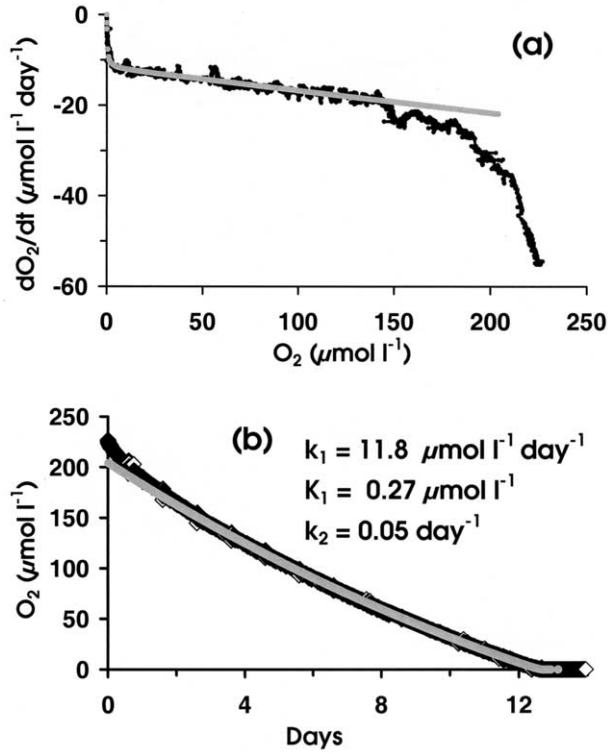
Fig. 11. (a) Representation of O_2 uptake rate as a function of dissolved O_2 for pulse 8. The gray line shows the stationary kinetics model, combining Monod and first-order rate laws. The initial transient appears as a region of rapidly decreasing uptake rate. (b) Evolution of O_2 concentration during pulse 8. The gray line represents the fitted model represented by Eqn. 1.

scheme of Fe(II) oxidation by DO therefore includes both homogeneous and heterogeneous reactions. Sorption of Fe(II) species on mineral surfaces is relatively rapid and can be considered at equilibrium (Tamura et al., 1980; Van Cappellen and Wang, 1996):

$$>X + Fe^{2+} \leftrightarrow >X - (Fe^{2+}). \qquad (7)$$
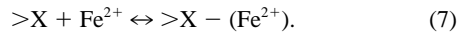
In this writing of the sorption reaction, $>X$ represents the unoccupied surface sites and $>X - (Fe^{2+})$ the occupied surface site. Following Tamura et al. (1980) and Van Cappellen and Wang (1996), it was assumed that the concentration of adsorbed Fe^{2+} may be calculated by a mass action law as follows:

$$[>X - (Fe^{2+})] = K_{Fe}^{s*}[Fe^{2+}][>X], \qquad (8)$$

where K_{Fe}^{s*} represents an apparent stability constant of the surface complexes and quantities in brackets are concentrations. As noted by Van Cappellen and Wang (1996), in case of a single sorbing phase, this apparent constant depends on pH, ionic strength and surface charge but in the case of a natural medium with a great variety of surface sites and stable major dissolved ions, it may be treated as an adjustable parameter. The surface of the diorite core indeed displays such a variety of mineral surfaces and Eqn. 8 was assumed to be applicable. In addition, it was assumed that the concentration of unoccupied

surface sites $[>X]$ was much larger than the concentrations of occupied surface sites $[>X - (Fe^{2+})]$ and of aqueous iron, $[Fe^{2+}]$. Eqn. 8 was therefore condensed into a linear relation, analogous to a distribution coefficient between solid and solution for Fe^{2+}:

$$[>X - (Fe^{2+})] = K_{Fe}[Fe^{2+}]. \qquad (9)$$

An order of magnitude estimate of the constant K_{Fe} can be determined by utilizing the data provided by Tamura et al. (1980). For Fe(III) hydroxides, these authors assign to the constant K_{Fe}^{s*} of Eqn. 8 a range of 8×10^{-4} to 3.3×10^{-3} mg^{-1} l at pH 6.5 and 25°C. The amount of sorbing minerals accessible to Fe^{2+} at the surface of the core is difficult to quantify. Observations of the core showed that alteration products were scarce at the surface of the fracture, although this surface was rough, with open mineral joints. The mass of sorbing minerals accessible to solution at the surface of the core was thus probably low—on the order of a few grams or less. The expected order of magnitude for K_{Fe} in our experimental conditions is therefore low, probably less than 10. The rate of the reaction of sorbed Fe(II) with DO,

$$4[>X - (Fe^{2+})] + O_2 + 10H_2O \rightarrow$$

$$4[>X] + 4Fe(OH)_3 + 8H^+ \qquad (10)$$
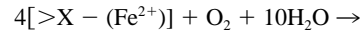
may be described by a simple bimolecular rate law, as supported by the works of Tamura et al. (1980) and Wehrli (1990):

$$\frac{d[>X - (Fe^{2+})]}{dt} = -k_d[>X - (Fe^{2+})][O_2], \qquad (11)$$

where k_d (mol^{-1} d^{-1}) is the bimolecular rate-law constant. The total rate of Fe(II) oxidation due to reaction with aqueous oxygen may thus be expressed as the sum of homogeneous and heterogeneous contributions, which are given by Eqns. 6 and 11, respectively. Also, taking into account Eqn. 9, following expression is obtained:

$$\frac{d[Fe(II)_{tot}]}{dt} = (1 + K_{Fe}) \frac{d[Fe_{2+}]}{dt}$$

$$= -\left\{ \frac{k_c}{[H^+]^2} + k_d K_{Fe} \right\}[Fe^{2+}][O_2]. \qquad (12)$$

Wehrli (1990) gives a numerical value for k_c at 25°C ($\sim 2 \times 10^{-9}$ mol L^{-1} d^{-1}). Data given in Tamura et al. (1980) indicate a probable range for k_d from 10^5 to $\sim 2 \times 10^7$ mol^{-1} d^{-1}. The form of Eqn. 12 is similar to that proposed by Tamura et al. (1980) in their study of catalyzed iron(II) oxidation. As mentioned above, this expression is first order in $[O_2]$ but has a time variable coefficient that is not compatible with the constancy of k_2 in Eqn. 1. Pyrite dissolution could account for such a stationary first-order contribution (Kamei and Ohmoto, 2000). From observations of pyrite dissolution in closed systems, these authors derived for the reaction

$$FeS_2(pyrite) + 3.5 O_2 + H_2O \Rightarrow Fe^{2+} + 2 SO_4^{2-} + 2 H^+$$

$$\qquad (13)$$
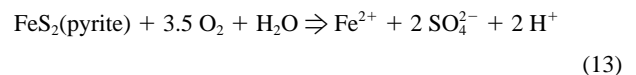
a first-order rate expression

$$\frac{d[FeS_2]}{dt} = -k_{Py}[O_2], \tag{14}$$

with a rate constant k_{Py} of approximately $10^{-5.3} \ m^{-2} \ s^{-1}$ at 25°C and pH = 5.7. This would be compatible with our experimental data if the reactive surface area of pyrite was around 300 cm^2, which seems rather high considering only macroscopic pyrite crystals were observed on the diorite core. However, microscopic iron sulfides are also probably present because SRB are plentiful (Table 5). Neal et al. (2001) observed that SRB were able to produce microscopic iron sulfides at the surface of hematite. The weak pH dependence of pyrite dissolution kinetics would explain the constancy of the first-order term k_2. Neglecting the oxidation reactions involving Mn(II) and combining Eqns. 1, 12, 13, and 14, leads to the following expression for the time derivative of DO:

$$\frac{d[O_2]}{dt} = -\frac{k_1[O_2]}{K_1 + [O_2]} - 3.5 \, k_{Py}^* \, [O_2]$$

$$- 0.25 \left\{ \frac{k_c}{[H^+]^2} + k_d K_{Fe} \right\} [Fe^{2+}][O_2] \tag{15}$$

where k_{Py}^* is equal to k_{Py} multiplied by the reactive surface area of pyrite. Eqn. 15, which is an elaborated form of the empirical Eqn. 1, shows that the evolution of DO is strongly coupled to the evolutions of Fe^{2+} and pH. As shown by the solution data (Fig. 7b), the reaction scheme for iron(II) should include source terms active in the absence of O$_2$. The high concentration of iron reducing bacteria (IRB) observed during the experiment (Tables 4 and 5, Fig. 9) points out Fe(III) respiration as one of the important iron(II) source terms (Lovley, 1993, 1994). This process may be schematically represented by the oxidation reaction of acetate by iron(III) hydroxide:

$$CH_3COO^- + 8Fe(OH)_{3ppt} + 15H^+ \rightarrow$$

$$2HCO_3^- + 20H_2O + 8Fe^{2+}. \tag{16}$$
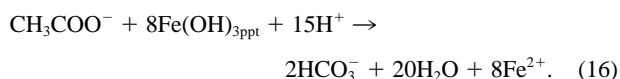
In addition to a suitable source of carbon, the major substrate for IRB is a mineral containing iron(III). Iron oxides and oxyhydroxides exist in fracture fillings and altered minerals (oligoclase) of the Äspö diorite (Banwart, 1994; Tullborg, 1995). Amorphous iron hydroxides are known to be more easily reduced than other iron oxyhydroxides (lepidocrocite, goethite, hematite) probably because of higher specific surface area (Ottow, 1969; Kostka et al., 1999). These minerals were, however, not individually identified on the fracture surface of the REX core and are therefore thought to occur as submicron crystals. The Eh-pH diagrams confirm that equilibrium with iron oxides or oxyhydroxides is reached (Fig. 5). Another hypothesis is that the main iron(III) substrate for IRB is composed of clay type minerals (Kostka et al., 1996), perhaps chlorites. Following Rittmann and VanBrisen (1996), a formulation for the rate law of reaction 16 was made by the use of a multiplicative-Monod form:

$$\frac{d[Fe^{2+}]}{dt} \propto \left(\frac{[CH_3COO^-]}{K_{acetate} + [CH_3COO^-]} \right) \left(\frac{[Fe(OH_{3ppt})]}{K_{FeIII} + [Fe(OH_{3ppt})]} \right),$$

$$\tag{17}$$

where $K_{acetate}$ and K_{FeIII} are the critical concentrations of the donor and acceptor substrates. In the present case, several arguments led to simplify this rate law to a constant form: (1) acetate concentrations (Table 3) remained at level, usually much greater than the typical range for critical concentrations of substrates that are usually low ($<<1 \ \mu mol \ L^{-1}$) (Rittmann and VanBriesen, 1996); the acetate related Monod factor in Eqn. 17 should therefore remain nearly constant; (2) for the same reason as for acetate substrate, the second factor in Eqn. 17 was assumed to be nearly constant; although the fracture surface contains few visible alteration products, iron(III) hydroxide concentration in the experimental vessel was certainly much larger than 1 $\mu mol \ L^{-1}$; and (3) the evolution of dissolved iron(II) is nearly linear during the final anoxic period (Fig. 7b). Taking into account the sorption reaction of Fe^{2+}, Eqn. 17 therefore simplifies to

$$(1 + K_{Fe}) \frac{d[Fe^{2+}]}{dt} = k_{1Fe}. \tag{18}$$

The order of magnitude given to k_{1Fe} (mol $L^{-1} \ d^{-1}$) should be consistent with the observed increase of dissolved iron during anoxic period (Fig. 7b) and correlated with the IRB population data (Tables 4 and 5). The high level of iron ($\sim 1 \ \mu mol \ L^{-1}$) maintained in solution during oxic periods supports the idea that iron(II) production through reaction 16 was active even when oxygen was present. Bacteria-promoted dissolution (Kalinowski et al., 2000) and, because in our experiment noticeable concentrations of organics are present in solution, reductive dissolution of iron(III) (hydr)oxides (Hering and Stumm, 1990; Suter et al., 1991) are also potential source terms for iron(II). However, they were neglected in this modeling approach. With these assumptions, an evolution equation for Fe^{2+} was obtained by combining Eqns. 12, 13, 14, and 18:

$$(1 + K_{Fe}) \frac{d[Fe^{2+}]}{dt} = -\left\{ \frac{k_c}{[H^+]^2} + k_d K_{Fe} \right\} [Fe^{2+}][O_2]$$

$$+ k_{Py}^*[O_2] + k_{1Fe}. \tag{19}$$

Corresponding equations for the evolution of hydrogen, carbon, calcium, calcite were elaborated. Processes involved in the evolution of the observed redox perturbations clearly involve the coupling of homogeneous and heterogeneous inorganic reactions, with microbial metabolism and result in states of dynamic equilibrium. Van Cappellen and Wang (1996) and Wang and Van Cappellen (1996) presented a detailed mechanistic modeling of the cycling of Fe and Mn at the seawater–sediment interface and they computed steady-state vertical profiles of major chemical species near this interface. This type of detailed modeling is not possible for our system for two reasons. First, the complete description of several surface processes, especially protonation/deprotonation reactions (Stumm, 1992) and sorption reactions for Fe(II) and Mn(II) (Smith and Jenne, 1991) require parameters (site densities, surface areas, equilibrium constants) that are coupled and cannot be easily bracketed for the diorite unless specific studies are conducted in sterile conditions. Second, the parameters individually describing the different kinetics relative to microbial activity are not sufficiently known unless specific culture studies are designed for potential substrates such as epidote or chlorite. However, taking into account available information (O$_2$ uptake kinetics, pH

Table 6. Rate law forms, units, and fitted values for the modeling of pulses P3 and P7 presented in Figures 12 and 13..

Process	Reactions	Rate law	Parameters	Pulse 3	Pulse 7
Reaction of Fe^{2+} with O_2	(4) (7) (10)	$\dfrac{d[Fe^{2+}]}{dt} = -\left\{ \dfrac{k_c}{[H^+]^2} + k_d K_{Fe} \right\} \dfrac{[Fe^{2+}][O_2]}{(1 + K_{Fe})}$	k_c (day^{-1}) k_d (mol^{-1} day^{-1}) K_{Fe}	1.7×10^{-9} 2×10^{7} 1	1.7×10^{-9} 2×10^{7} 1
Oxidation of pyrite	(13)	$\dfrac{d[FeS_2]}{dt} = -k_{Py}^*[O_2]$	k_{Py}^* (d^{-1})	2.5×10^{-2}	2.5×10^{-2}
Aerobic respiration	(2)	$\dfrac{d[O_2]}{dt} = -\dfrac{k_1[O_2]}{(K_1 + [O_2])}$	k_1 (mol L^{-1} d^{-1}) K_1 (mol L^{-1})	2.8×10^{-5} 2×10^{-7}	9.6×10^{-6} 2×10^{-7}
Fe(III) respiration	(18)	$(1 + K_{Fe})\dfrac{d[Fe^{2+}]}{dt} = k_{1Fe}$	k_{1Fe} (mol L^{-1} d^{-1})	3×10^{-7}	5×10^{-6}
Calcite dissolution	(3)	$\dfrac{d[Calcite]}{dt} = -k_{cal}\left(1 - \dfrac{[Ca^{2+}][HCO_3^-]}{[H^+]K_c^*}\right)$	k_{cal} (mol L^{-1} d^{-1}) K^*c (mol L^{-1})	1×10^{-6} 447	7×10^{-6} 447

and Eh evolutions, dissolved iron concentration) and major processes presently identified (microbial respiration, calcite dissolution, iron(II) oxidation, pyrite dissolution) a simplified simulation of this dynamic system can be conducted. In the modeling presented here, it was assumed that transport processes between different parts of the core surface were not limiting and the aim was to qualitatively reproduce the main independent signals obtained during the experiments— that is, temporal evolutions in pH and Eh. The following processes were included: (1) equilibrium aqueous chemical speciation among H^+, OH^-, HCO_3^-, CO_3^-, H_2CO_3; (2) calcite dissolution or precipitation (reaction 3). The rate law selected for this reaction was

$$\frac{d[Calcite]}{dt} = -k_{cal}\left(1 - \frac{[Ca^{2+}][HCO_3^-]}{[H^+]K_c^*}\right), \qquad (20)$$

where k_{cal} is a rate constant and K_c^* the apparent equilibrium constant for reaction 3; (3) aerobic and iron (III) respiration processes (reactions 2 and 16); (4) homogeneous and heterogeneous oxidation of iron(II) by O_2(aq) (reactions 4 and 10); and (5) pyrite oxidation by O_2(aq) (reaction 13).

Table 6 summarizes rate law forms selected for each process and major parameters. The Eh value was computed from pH and Fe^{2+} by a correlation similar to that found by Grenthe et al. (1992) for Eh field measurements, corresponding to a hypothetical equilibrium with an iron (III) hydroxide,

$$Fe(OH)_{3ppt} + 3H^+ + e^- \leftrightarrow Fe^{2+} + 3H_2O. \qquad (21)$$

Although the concentration of Fe^{2+} during DO pulses is governed by kinetics (Eqn. 19), the instantaneous Eh value was computed with following rearranged form of the mass action law for reaction 21:

$$Eh_{SHE}(25°C) = \frac{RT}{F}(\log K_s - 3pH - \log[Fe^{2+}]), \quad (22)$$

where K_S is the equilibrium constant for reaction 21, R the gas constant, F the Faraday constant and T the temperature in K. The validity of relation (22) implies that the precipitation of the iron(III) hydroxide at the Pt electrode is fast. The aqueous speciation of iron(II) was restricted to the species Fe^{2+}. The ionic strength of the aqueous solution was nearly constant

($\sim$0.55 mol/L) and activity corrections were implicitly made by taking into account the apparent equilibrium constants deduced from a speciation run performed with CHESS 2.4 and the b-dot activity model (Van der Lee, 1998). Mass balances and temporal variations derived from processes and rate laws listed in Table 6 were numerically solved. Comparison of model predictions with observations for pulses P3 and P7 are shown in Figures 12 and 13. The predicted trends for Eh and pH are in good agreement with observations, showing that this simple model includes major processes that are active in the experiment. As mentioned above, several processes that were not explicitly included in the present approach explain some of the discrepancies between data and model in Figures 12 and 13. For example, the incorporation of Mn(II)/Mn(IV) redox and Mn(IV) respiration reactions in the model would be consistent with Mn solution data (Table 3) and should slightly modify pH and Eh evolutions in the anoxic region (Davies and Morgan, 1989; Smith and Jenne, 1991; Lovley, 1993, 1994; Van Cappellen and Wang, 1996). Solution pH is also probably influenced by the dissolved organic molecules present, and this should be included in future such modeling efforts.

In both simulations, the initial aqueous iron concentration was taken equal to 0.5 μmol L^{-1} and the initial total carbonate concentrations was taken near experimental values (Table 3): 0.29 mmol L^{-1} for pulse P3, 1.1 mmol L^{-1} for pulse P7. Kinetic constants related to reactions (13) (k_{Py}^*, pyrite oxidation) and (2) (k_1, K_1, aerobic respiration) were first estimated from the experimental DO signal by the procedure described to derive Eqn. 1 and then were more finely tuned during the simultaneous solution of all equations. The kinetic constant related to Eqn. 18 (k_{1Fe}, iron(III) respiration) was derived by fitting the rate of Eh decrease in the anoxic region after each pulse. For pulse P3, the value taken for the constant k_{1Fe} was also consistent with measured iron concentrations at the end of the first anoxic period. The rate constant for calcite dissolution (k_{cal}) was adjusted to simultaneously moderate the pH drop in oxic conditions and reproduce correctly the pH increase in anoxic conditions. The rate constant k_c in Eqn. 12 was taken from Wehrli (1990). The equilibrium constant K_S for reaction 21, the distribution coefficient K_{Fe} of reaction 9, and the rate constant k_d of reaction 11 were set to reproduce correctly the initial Eh plateau. This was made by a preliminary direct
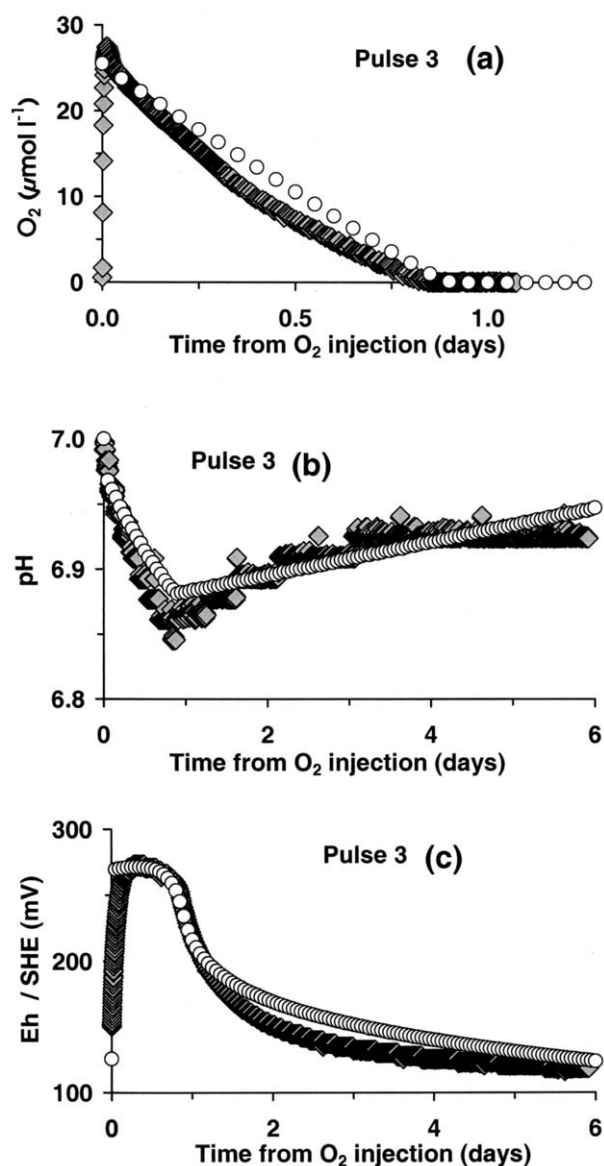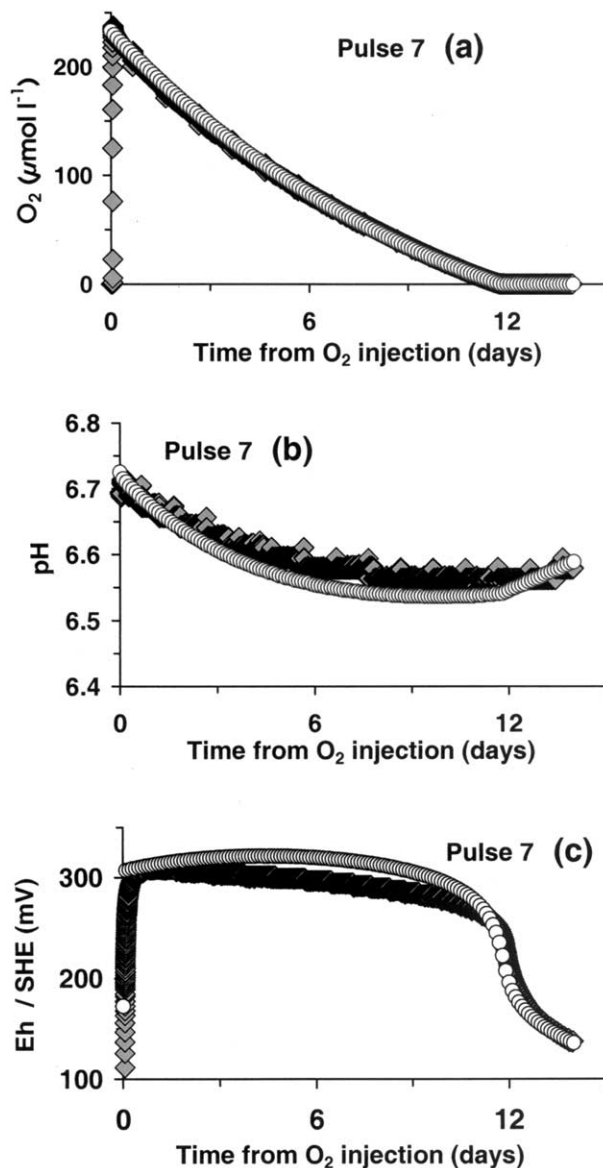
Fig. 12. Comparison of experimental data (diamonds) and simulation results (circles) for pulse 3. (a) Dissolved O_2 vs. time. (b) pH vs. time. (c) Eh vs. time. Parameters selected for the simulation are listed in Table 6 and discussed in the text.

Fig. 13. Comparison of experimental data (diamonds) and simulation results (circles) for pulse 7. (a) Dissolved O_2 vs. time. (b) pH vs. time. (c) Eh vs. time. Parameters selected for the simulation are listed in Table 6 and discussed in the text.

simulation of the Eh signal, using experimental values of DO, pH, and an explicit finite difference scheme to qualitatively reproduce this initial Eh plateau. This trial and error procedure confirmed that the proper ranges for k_d and K_{Fe} were respectively from 10^6 to 5×10^7 mol^{-1} d^{-1} and less than 5. Final adjustment of model parameters led to the same set of values for K_{Fe} (1.0) and k_d (2×10^7 mol^{-1} d^{-1}) for pulse P3 and pulse P7. The low value found for K_{Fe} confirms the scarcity of sorbing minerals at the surface of the core. These sorbing minerals act to catalyze DO consumption by Fe(II) but do not represent, in our experimental conditions, an important reservoir of Fe(II). Both simulations required close values for K_S— that is, 16.8 for pulse 3, 16.7 for pulse 7. As quoted by Grenthe
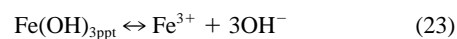
et al. (1992) and Langmuir and Whittemore (1971), the equilibrium constant K_s^* for the reaction

$$Fe(OH)_{3ppt} \leftrightarrow Fe^{3+} + 3OH^- \qquad (23)$$

falls in the range $37.3 < pK_s^* < 44.1$ for amorphous ferric hydroxide to crystalline goethite. The value obtained in both simulations for K_S yields a pK_s^* of $\sim$38, in good agreement for a typical amorphous iron (III) hydroxide. Consequently, conclusions reached by Grenthe et al. (1992) for Eh potentials measured in anoxic granitic groundwaters near equilibrium seem also to be valid for our replica experiment. The Eh-pH diagram of Fig. 5b suggests, however, that after a long anoxic period the solution came to equilibrium with a crystalline

phase, goethite. This observation is supported by Langmuir (1969) and Langmuir and Whittemore (1971), who found that the stability of iron hydroxide increases upon ageing and eventually reaches the pK_s of goethite.

The sets of parameters selected for the simulation of pulse P3 and pulse P7 differ from one another principally in the values given to k_{cal} (calcite dissolution kinetics, reaction 3), k_1 (aerobic respiration, reaction 2), and k_{1Fe} Fe(III) respiration (reaction 16). In addition, simulations showed that the pH evolution was rather sensitive to the value set for these three parameters. The higher value taken by k_{1Fe} for pulse P7 is consistent with the development of IRB between pulses P1 and P7, as shown in Fig. 10 and Table 4. The higher value of k_{cal} required in the simulation of pulse 7 could be correlated to (1) the influence of the pH decrease from pulse P3 to pulse P7; (2) an increase of the reactive surface of calcite due to intense etching (Fig. 10a); and (3) an enhancement of the dissolution kinetics of calcite due to the increase of organic ligands in solution (Fig. 7d). The rate-law form selected for calcite dissolution–precipitation kinetics (Eqn. 20) is a simplified version of the complete expression determined by Plummer et al. (1978)

$$\text{Rate} = \alpha_1 a_{H^+} + \alpha_2 a_{H_2CO_3^*} + \alpha_3 a_{H_2O} - \alpha_4 a_{Ca^{2+}} a_{HCO_3^-}, \tag{24}$$

where α_1, α_2, α_3 are temperature-dependent first-order rate constants, α_4 is a function of both temperature and PCO_2, and $H_2CO_3^*$ is $CO_2(aq) + H_2CO_3^0$. Rewriting Eqn. 24 as follows,

$$\text{Rate} = \alpha_1 a_{H^+}\left(1 - \frac{\alpha_4 a_{Ca^{2+}} a_{HCO_3^-}}{\alpha_1 a_{H^+}}\right) + \alpha_2 a_{H_2CO_3^*} + \alpha_3 a_{H_2O}$$
$$\tag{25}$$

and comparing with Eqn. 20 shows that this more complete rate law-form accounts well for the increase of calcite dissolution rate k_{cal} from pulses P3 and P7 by a factor between 3 and 10, as a consequence of solution acidification. The value of k_{cal} taken in our computations corresponds to a surface area of calcite in the range of 0.01 to 0.1 m², which is compatible with the observed abundance of calcite on the core surface. The evolution of k_1 between pulse P3 and pulse P7 is not fully understood but could be due to the influence of strict aerobic bacteria that were initially present in the apparatus. The alternating oxic and anoxic experimental conditions would have favored facultative aerobes, whereas strict aerobes might have become inactive after pulse P3, resulting in the decrease of rate constant k_1. Finally, the rate coefficient for pyrite oxidation (k_{Py}^*) is similar for the two pulses. The value taken by k_{Py}^* would correspond, following Kamei and Ohmoto (2000) to a surface area of ~0.05 m² for dissolving pyrite. This value of surface area indicates a probable contribution of microscopic pyrite or iron sulfide crystals because observable pyrite crystals are scarce on the diorite core. In addition, a fraction of the reactive minerals are probably situated under the immediate core surface and are not evident from a visual examination of the core surface. This was true at least for calcite, as shown by SEM observations of corroded "internal" surfaces (only accessible through channels) of diorite fragments detached from the core. In a real fracture medium, the specific role of transport modes and features could play an important role that was not addressed by our experiments and modeling.

This leads us to another aspect of the replica REX experiment, namely its role as a mock-up. From the above presentation, it appears that this experiment provides quantitative information on the succession of phenomena and related processes occurring, as well as the time periods involved. This experiment also gives guidelines for field investigations, identifying some relevant parameters to measure or monitor. The major discrepancies between the replica experiment and actual field conditions are related to available microbial substrates: an additional internal carbon source is present in the setup; and H_2 and CH_4 fluxes observed in the field (Kotelnikova and Pedersen, 1999a) were not properly reproduced in the experiment. These discrepancies would cause some microorganisms identified in the field not to develop, especially bacteria having their energy source in reactions between O_2 and H_2 or CH_4. On the other hand, because of the extra carbon source supplied by the setup, heterotrophic or fermentative bacteria development was favored in the replica experiment. A good agreement in trends observed for bacterial populations was nevertheless found by Kotelnikova and Pedersen (1999b) by comparison with the in situ experiment. This is especially striking for IRB, for which explosive development followed low oxygen pulses in both experiments and some decrease occurred with higher DO pulses. The microbial numbers for IRB at the surface of the core were also in good agreement (~2 × 10⁴ cells cm⁻² for both experiments).

Finally, the replica experiment contributed to the elaboration of a more precise and detailed analysis of what is often called the "buffering capacity" of a geological medium with respect to redox perturbations. Static quantities related to solution or solid phase composition are not relevant because it is shown that the main processes involved are linked to the cycling of iron and manganese by coupled inorganic/organic phenomena at the solid/solution interface. Microbial populations, especially IRB, are robust and able to adapt to both aerobic and anaerobic conditions. A more refined and operational concept of buffering capacity should include at least two types of bacterial populations (aerobic + IRB), quantify the fluxes of their substrates in the system and characterize the interfacial properties of available Fe and Mn hydroxides and microscopic iron sulfide phases.

5. CONCLUSIONS

The characteristic time for oxygen uptake in a simulated fracture in deep granite is found to range from 1 to 4 weeks in our experimental conditions (15°C), and at least 2 months are necessary to progress from anoxic to reducing conditions. The reaction path is shown to involve equilibrium of the solution with respect to iron (hydr)oxides. However, complete return to chemical equilibrium was not achieved during the experiment, mainly because of the rate limited dissolution of mineral phases.

These results will be useful to elaborate a simplified but dynamical conceptual model of the "redox buffering capacity" in a granite medium and therefore identify relevant parameters to be measured at a disposal site. Data and modeling show that coupled organic/inorganic processes involving aerobic bacteria and IRB govern major redox evolutions. Consequently, data pertaining to the types, availability, and fluxes of bacterial

substrates are crucial for the prediction of postclosure redox conditions in a waste disposal site. However, additional research effort is necessary to more fully describe the interfacial reactions occurring between iron and manganese hydroxides, aqueous solutions and biofilm. The fact that quasi steady-state kinetics were measured for O_2 uptake suggests that the pH dependence of relevant interfacial processes is weak, between pH 6 and 8.

In addition, the replica experiment has a methodologic interest with respect to the development of in situ experiments for High Level Nuclear Waste disposal research. This approach is powerful and seems adapted for geochemical systems with a limited spatial extension (<1 m). The experimental artefacts present in our experiments, which were related to an imprecise control of bacterial substrates, can probably be overcome. Finally, it was shown that the conception of in situ geochemical experiments (e.g., related to corrosion or alteration of materials) must include the effect of bacteria as an integral part of the experiment.

Associate editor: M. A. Machesky

REFERENCES

Adler H. H. (1974) Concepts of uranium-ore formation in reducing environments in sandstones and other sediments. In *Formation of Uranium Deposits*, 141–168. IAEA.

Alaux-Negrel G.(1991) Etude de l'évolution des eaux profondes en milieux granitiques et assimilés. Comportement deséléments en traces. PhD Thesis. University of Paris VII.

Allen M. J., Taylor R. H., and Geldreich E. E. (1980) The occurrence of microorganisms in water main encrustations. *J. Am. Water Works Assoc.* **82,** 614–625.

BanfieldJ. F.NealsonK. H.,eds. (1997) Geomicrobiology: Interactions between Microbes and Minerals. Reviews in Mineralogy 35. Mineralogical Society of America.

Banwart S. (1994) SKB International Cooperation Report 94-13 Proceedings of the Äspö International Geochemistry Workshop, June 2–3, 1994. Äspö Hard Rock Laboratory.

Banwart S., Gustafsson E., Laaksoharju M., Nilsson A.-C., Tullborg E.-L., and Wallin B. (1994) Large-scale intrusion of shallow water into a vertical fracture zone in crystalline bedrock: Initial hydrochemical perturbation during tunnel construction at the Äspö Hard Rock Laboratory, south-eastern Sweden. *Water Res. Res.* **30,** 1747–1763.

Barns S. M. and Nierzwicki-Bauer S. A. (1997) Microbial diversity in ocean, surface and subsurface environments. In *Geomicrobiology: Interactions between Microbes and Minerals,* Vol. 35 (eds. J. F. Banfield and K. H. Nealson), 35–79 Reviews in Mineralogy 35. Mineralogical Society of America.

Bethke C. (1994) *The Geochemist's Workbench. Version 2.0, Users Guide*. University of Illinois.

Bottomley D. J., Gascoyne M., and Kamineni D. C. (1990) The geochemistry, age and origin of groundwater in a mafic pluton, East Bull Lake, Ontario, Canada. *Geochim. Cosmochim. Acta* **54,** 993–1008.

Buffle J. and Stumm W. (1993) General chemistry of aquatic systems. In *Chemical and Biological Regulation of Aquatic Systems* (eds. J. Buffle and R. De Vitre), 1–42. Lewis Publishers.

Chapman N., McKinley I., and Hill M. (1987) *The Geological Disposal of Nuclear Waste*. Wiley.

Cross J. E., Haworth A., Neretnieks I., Sharland S. M., and Tweed C. J. (1991) Modelling of redox front and uranium movement in a uranium mine at Pocos de Caldas. *Radiochim. Acta* **52/53,** 445–451.

Davies S. H. R. and Morgan J. J. (1989) Manganese (II) oxidation kinetics on metal oxide surfaces. *J. Colloid Interface Sci.* **129,** 63–77.

De Vitre R., Sulzberger B., and Buffle J. (1993) Transformations of iron at redox boundaries. In *Chemical and Biological Regulation of Aquatic Systems* (eds. J. Buffle and R. De Vitre), 89–135. Lewis Publishers.

Diem D. and Stumm W. (1984) Is dissolved Mn $^{2+}$ being oxidized by O_2 in absence of Mn-bacteria or surface catalysts? *Geochim. Cosmochim. Acta* **48,** 1571–1573.

Fürrer G. and Wehrli B. (1996) Microbial reactions, chemical speciation and multicomponent diffusion in porewaters of a eutrophic lake. *Geochim. Cosmochim. Acta* **60,** 2333–2346.

Gascoyne M. (1997) Evolution of redox conditions and groundwater composition in recharge–discharge environments on the Canadian shield. *Hydrogeol.* **5,** 4–18.

Grenthe I., Stumm W., Laaksoharju M., Nilsson A.-C., and Wikberg P. (1992) Redox potentials and redox reactions in deep groundwater systems. *Chem. Geol.* **98,** 131–150.

Grimaud D., Beaucaire C., and Michard G. (1990) Modelling the evolution of ground waters in a granite system at low temperature: The Stripa ground waters, Sweden. *Appl. Geochem.* **5,** 515–525.

Hering J. G. and Stumm W. (1990) Oxidative and reductive dissolution of minerals. In Mineral–water interface geochemistry Vol. 23 (ed. P. H. Ribbe), 427–465. Reviews in Mineralogy. Mineralogical Society of America.

Junta J. L. and Hochella Jr. M. F. (1994) Manganese(II) oxidation at mineral surfaces: A microscopic and spectroscopic study. *Geochim. Cosmochim. Acta* **58,** 4985–4999.

Kalinowski B. E., Liermann L. J., Givens S., and Brantley S. L. (2000) Rates of bacteria-promoted solubilization of Fe from minerals: A review of problems and approaches. *Chem. Geol.* **169,** 357–370.

Kamei G. and Ohmoto H. (2000) The kinetics of reactions between pyrite and O_2-bearing water revealed from in situ monitoring of D.O., Eh and pH in a closed system. *Geochim. Cosmochim. Acta* **64,** 2585–2601.

Kostka J. E., Stucki J. W., Nealson K. H., and Wu J. (1996) Reduction of structural Fe(III) in smectite by a pure culture of Shewanella putrefaciensstrain MR-1. *Clays Clay Miner.* **44,** 522–529.

Kostka J. E., Wu J., Nealson K. H., and Stucki J. W. (1999) The impact of structural Fe(III) reduction by bacteria on the surface chemistry of smectite clay minerals. *Geochim. Cosmochim. Acta* **63,** 3705–3713.

Kotelnikova S. and Pedersen K. (1999a) *Microbial Oxygen Reduction in the Äspö Tunnel: The Microbe-Rex Project*. Swedish Nuclear Fuel Waste Management SKB-TR 99-17.

Kotelnikova S. and Pedersen K. (1999b) *Microbial Oxygen Consumption during the REX Field Experiment* Report SKB-IPR-00-19. Stockholm, Sweden.

Laaksoharju M., Tullborg E.-L., Wikberg P., Wallin B, and Smellie J. (1999) Hydrogeochemical conditions and evolution at the Äspö HRL, Sweden. *Appl. Geochem.* **14,** 835–859.

Langmuir D. (1969) *The Gibbs Free Energies of Substances in the System $Fe-O_2-H_2O-CO_2$ at 25°C*. Professional Paper 650-B. U.S. Geological Survey.

Langmuir D.and Whittemore D. O. (1971) Variations in the stability of precipitated ferric oxyhydroxides. In *Nonequilibrium Systems in Natural Water Chemistry*. (ed. R. F. Gould), pp. 209-234. Adv. Chem. Ser. 106.

Lovley D. R. (1993) Dissimilatory metal reduction. *Annu. Rev. Microbiol.* **47,** 263–290.

Lovley D. R. (1994) Microbial reduction of iron, manganese, and other metals. *Adv. Agron.* **54,** 175–231.

Lovley D. R. and Chapelle F. H. (1995) Deep subsurface microbial processes. *Rev. Geophys.* **33,** 365–381.

Mahara Y., Igarashi T., Hasegawa T., Miyakawa K., Tanaka Y., and Kiho K. (2001) Dynamic changes in hydrogeochemical conditions caused by tunnel excavation at the Äspö Hard Rock Laboratory (HRL), Sweden. *Appl. Geochem.* **16,** 291–315.

Malmström M., Banwart S., Lewenhagen J., Duro L., and Bruno J. (1996) The dissolution of biotite and chlorite at 25°C in the near-neutral pH region. *J. Contaminant Hydrol.* **21,** 201–213.

Millero F. (1985) The effect of ionic interactions on the oxidation of metals in natural waters. *Geochim. Cosmochim. Acta* **49,** 547–554.

Millero F. J., Hubinger S., Fernandez M., and Garnett S. (1987a) Oxidation of H_2S in seawater as a function of temperature, pH and ionic strength. *Environ. Sci. Technol.* **21,** 439–443.

Millero F. J., Sotolongo S., and Izaguirre M. (1987b) The oxidation kinetics of Fe(II) in seawater. *Geochim. Cosmochim. Acta* **51,** 793–801.

Neal A. L., Techkarnjanaruk S., Dohnalkova A., McCready D., Peyton B. M., and Geesey G. G. (2001) Iron sulphides and sulphur species produced at hematite surfaces in the presence of sulphate-reducing bacteria. *Geochim. Cosmochim. Acta* **65,** 223–235.

Nealson K. H. and Saffarini D. (1994) Iron and manganese in anaerobic respiration: Environmental significance, physiology, and regulation. *Annu. Rev. Microbiol.* **48,** 311–343.

Nordstrom D. K., Ball J. W., Donahoe R. J., and Whittemore D. (1989) Groundwater chemistry and water–rock interactions at Stripa. *Geochim. Cosmochim. Acta* **53,** 1727–1740.

Ottow J. C. G. (1969) The distribution and differentiation of iron-reducing bacteria in clay soils. *Zentralbl. Bakteriol. Parasitenkd Infekstionskr Hyg.* **124,** 600–615.

Pedersen K. (1996) Investigations of subterranean bacteria in deep crystalline bedrock and their importance for the disposal of nuclear waste. *Can. J. Microbiol.* **42,** 382–391.

Pedersen K. (1997) Microbial life in deep granitic rock. *FEMS Microbiol. Rev.* **20,** 399–414.

Pirhonen V.and Pitkänen, P. (1991) Redox Capacity of Crystalline Rocks: Laboratory Studies under 100 bar Oxygen Gas Pressure. Technical Report 91-55, SKB, Stockholm, Sweden.

Plummer L. N., Wigley T. M. L., and Parkhurst D. L. (1978) The kinetics of calcite dissolution in CO_2-water systems at 5°C to 60°C and 0.0 to 1.0 atm CO_2. *Am. J. Sci.* **278,** 179–216.

Puigdomenech I., Banwart S. A., Bateman K., Griffault L., Gustafsson E., Hama K., Kotelnikova S., Lartigue J.-E., Michaud V., Milodowski A. E., Morosini M., Pedersen K., Rivas-Perez J., Trotignon L., Tullborg E.-L., West J. M., and Yoshida H. (1998) *Äspö Hard Rock Laboratory—Redox Experiment in Detailed Scale (REX): First Project Status Report.* SKB IC Report 99-01.

Puigdomenech I., Trotignon L., Kotelnikova S., Pedersen K., Griffault L., Michaud V., Lartigue J.-E., Hama K., Yoshida H., West J. M., Bateman K., Milodowski A. E., Banwart S. A., Rivas Perez J., and Tullborg E. L. (1999) O_2 consumption in a granitic environment. In *Scient. Basis Nucl. Waste Manag.,* Vol. 23 (eds. R. W. Smith and D. W. Shoesmith), 179–184 Symp. Proc. Vol. 608. Mat. Res. Soc.

Puigdomenech I., Ambrosi J.-P., Eisenlohr L., Lartigue J.-E., Banwart S., Bateman K, Milodowski A. E., West J. M., Griffault L., Gustafsson E., Hama K., Yoshida H., Kotelnikova S., Pedersen K., Michaud V., Trotignon L., Rivas Perez J., and Tullborg E.-L. (2001) O_2 Depletion in Granitic Media: The REX Project. SKB Technical Report TR-01-05.

Rittmann B. E. and VanBriesen J. M. (1996) Microbiological processes in reactive modelling. In *Reactive Transport in Porous Media,* Vol. 34 (ed. P. H. Ribbe), 311–334. Mineralogical Society of America Reviews in Mineralogy 34.

Rosing M. T. (1993) The buffering capacity of open heterogeneous systems. *Geochim. Cosmochim. Acta* **57,** 2223–2226.

SKB (1995) *General Siting Study 95: Siting of a Deep Repository for Spent Nuclear Fuel.* Svensk Kärnbränslehantering AB.

Smith R. W. and Jenne E. A. (1991) Recalculation, evaluation and prediction of surface complexation constants for metal adsorption on iron and manganese oxides. *Environ. Sci. Technol.* **25,** 525–531.

Strömberg B. and Banwart S. (1994) Kinetic modelling of geochemical processes at the Aitik mining waste rock site in northern Sweden. *Appl. Geochem.* **9,** 583–595.

Stumm W. (1992) *Chemistry of the Solid–Water Interface.* Wiley.

Stumm W. and Lee G. F. (1961) Oxygenation of ferrous iron. *Industr. Eng. Chem.* **53,** 143–146.

Stumm W. and Morgan J. J. (1996) *Aquatic Chemistry..* Wiley.

Sung W. and Morgan J. J. (1980) Kinetics and product of ferrous iron oxygenation in aqueous systems. *Environ. Sci. Technol.* **14,** 561–568.

Suter D., Banwart S., and Stumm W. (1991) Dissolution of hydrous iron (III) oxides by reductive mechanisms. *Langmuir* **7,** 809–813.

Tamura H., Goto K., and Nagayama M. (1976) The effect of ferric hydroxide on the oxygenation of ferrous ions in neutral solution. *Corrosion Sci.* **16,** 197–207.

Tamura H., Kawamura S., and Nagayama M. (1980) Acceleration of the oxidation of Fe $^{2+}$ ions by Fe(III)-oxyhydroxides. *Corrosion Sci.* **20,** 963–971.

Thauer R. K. and Morris J. G. (1984) Metabolism of chemotrophic anaerobes: Old and new aspects. In *The Microbe: Part 2* (eds. D. P. Kelly and N. G. Carr), 123–168. Cambridge University Press.

Tullborg E.-L.(1995) Mineralogical and Chemical Data on Rocks and Fracture Minerals from Äspö. Äspö HRL Technical Note 25-95-07g. SKB.

Turpault M.-P.and Trotignon L.(1992) Experimental interaction between a granite wall and flowing aerated water. In *Proceedings of the 7th International Symposium on Water–Rock Interaction* (eds. Y. K. Kharaka and A. S. Maest), pp. 847–850. A. A. Balkema, Rotterdam.

Van Cappellen P. and Gaillard J.-F. (1996) Biogeochemical dynamics in aquatic sediments. *In Reactive Transport in Porous Media*, 335–376. Mineralogical Society of America Reviews in Mineralogy 34.

Van Cappellen P. and Wang Y. (1996) Cycling of iron and manganese in surface sediments: A general theory for the coupled transport and reaction of carbon, oxygen, nitrogen, sulfur, iron and manganese. *Am. J. Sci.* **296,** 197–243.

Van der Lee J.(1998) Thermodynamic and Mathematical Concepts of CHESS. Technical Report LHM/RD/98/39, CIG, Ecole des Mines de Paris.

Wang Y. and Van Cappellen P. (1996) A multicomponent reactive transport model of early diagenesis: Application to redox cycling in coastal marine sediments. *Geochim. Cosmochim. Acta* **60,** 2993–3014.

Wehrli B. (1990) Redox reactions of metal ions at mineral surfaces. In *Aquatic Chemical Kinetics:Reaction Rates of Processes in Natural Waters* (ed. W Stumm), 324–327 Wiley Interscience.

Wersin P., Spahiu K., and Bruno J. (1994) *Time Evolution of Dissolved Oxygen and Redox Conditions in a HLW Repository.* SKB Technical Report 94-02.

White A. F. and Peterson M. L. (1996) Reduction of aqueous transition metal species on the surfaces of Fe(II)-containing oxides. *Geochim. Cosmochim. Acta* **60,** 3799–3814.

White A. F. and Yee A. (1985) Aqueous oxidation-reduction kinetics associated with coupled electron-cation transfer from iron-containing silicates at 25°C. *Geochim. Cosmochim. Acta* **49,** 1263–1275.

Wikberg P. (1985) The assessment of reducing conditions at depth in granitic rock. In *Scientific Basis for Nuclear Waste Management* (ed. L. O. Werme), 137–144. Symposium Proceedings Vol. 50, Materials Research Society, Pittsburgh.

Williamson M. A. and Rimstidt J. D. (1994) The kinetics and electrochemical rate-determining step of aqueous pyrite oxidation. *Geochim. Cosmochim. Acta* **58,** 5443–5454.

Winberg A., Andersson P., Hermanson J., Stenberg L.Results of the SELECT Project: Investigation Programme for Selection of Experimental Sites for the Operational Phase. 1996Progress Report HRL-96-01. Swedish Nuclear Fuel Waste Manag.